

Article

# Electrochemical Corrosion of Titanium and Titanium Alloys Anodized in H<sub>2</sub>SO<sub>4</sub> and H<sub>3</sub>PO<sub>4</sub> Solutions

Jesús Manuel Jáquez-Muñoz <sup>1,\*</sup>, Citlalli Gaona-Tiburcio <sup>1</sup>, José Chacón-Nava <sup>2</sup>, Jose Cabral-Miramontes <sup>1</sup>, Demetrio Nieves-Mendoza <sup>3</sup>, Erick Maldonado-Bandala <sup>3</sup>, Anabel D. Delgado <sup>2</sup>, Juan Pablo Flores-De los Rios <sup>4</sup>, Patrizia Bocchetta <sup>5</sup> and Facundo Almeraya-Calderón <sup>1,\*</sup>

- <sup>1</sup> Universidad Autonoma de Nuevo Leon, FIME-Centro de Investigación e Innovación en Ingeniería Aeronáutica (CIIA), Av. Universidad s/n, Ciudad Universitaria, San Nicolás de los Garza 66455, Mexico; citlalli.gaonatbr@uanl.edu.mx (C.G.-T.); jose.cabralmr@uanl.edu.mx (J.C.-M.)
- <sup>2</sup> Department of Metallurgy and Structural Integrity, Centro de Investigación en Materiales Avanzados (CIMAV), Miguel de Cervantes 120, Complejo Industrial Chihuahua, Chihuahua 31136, Mexico; jose.chacon@cimav.edu.mx (J.C.-N.); anabel.delacruz@cimav.edu.mx (A.D.D.)
- <sup>3</sup> Facultad de Ingeniería Civil, Universidad Veracruzana, Xalapa 91000, Mexico; dnieves@uv.mx (D.N.-M.); erimaldonado@uv.mx (E.M.-B.)
- <sup>4</sup> Department Metal-Mechanical, Tecnológico Nacional de México-Instituto Tecnológico de Chihuahua, Av. Tecnológico 2909, Chihuahua 31130, Mexico; juan.fd@chihuahua.tecnm.mx
- <sup>5</sup> Department of Innovation Engineering, University of Salento, via per Monteroni, 73100 Lecce, Italy; patrizia.bocchetta@unisalento.it
- \* Correspondence: jesus.jaquezmn@uanl.edu.mx (J.M.J.-M.); facundo.almerayaald@uanl.edu.mx (F.A.-C.)



**Citation:** Jáquez-Muñoz, J.M.; Gaona-Tiburcio, C.; Chacón-Nava, J.; Cabral-Miramontes, J.; Nieves-Mendoza, D.; Maldonado-Bandala, E.; Delgado, A.D.; Flores-De los Rios, J.P.; Bocchetta, P.; Almeraya-Calderón, F. Electrochemical Corrosion of Titanium and Titanium Alloys Anodized in H<sub>2</sub>SO<sub>4</sub> and H<sub>3</sub>PO<sub>4</sub> Solutions. *Coatings* **2022**, *12*, 325. <https://doi.org/10.3390/coatings12030325>

Academic Editor: Yong X. Gan

Received: 7 February 2022

Accepted: 20 February 2022

Published: 1 March 2022

**Publisher's Note:** MDPI stays neutral with regard to jurisdictional claims in published maps and institutional affiliations.



**Copyright:** © 2022 by the authors. Licensee MDPI, Basel, Switzerland. This article is an open access article distributed under the terms and conditions of the Creative Commons Attribution (CC BY) license (<https://creativecommons.org/licenses/by/4.0/>).

**Abstract:** Titanium and its alloys have superior electrochemical properties compared to other alloy systems due to the formation of a protective TiO<sub>2</sub> film on metal surfaces. The ability to generate the protective oxide layer will depend upon the type of alloy to be used. The aim of this work was to characterize the electrochemical corrosion behavior of titanium Ti-CP2 and alloys Ti-6Al-2Sn-4Zr-2Mo, Ti-6Al-4V, and Ti Beta-C. Samples were anodized in 1 M H<sub>2</sub>SO<sub>4</sub> and H<sub>3</sub>PO<sub>4</sub> solutions with a current density of 0.025 A/cm<sup>2</sup>. Electrochemical tests on anodized alloys were carried out using a three-electrode cell and exposed in two electrolytes, i.e., 3.5% wt. NaCl and 3.5% wt. H<sub>2</sub>SO<sub>4</sub> solutions at room temperature. Scanning electron microscopy (SEM) was used to observe the morphology of anodized surfaces. The electrochemical techniques used were cyclic potentiodynamic polarization (CPP) and electrochemical noise (EN), based on the ASTM-G61 and G199 standards. Regarding EN, two methods of data analysis were used: the frequency domain (power spectral density, PSD) and time-frequency domain (discrete wavelet transform). For non-anodized alloys, the results by CCP and EN indicate icorr values of ×10<sup>-6</sup> A/cm<sup>2</sup>. However, under anodizing conditions, the icorr values vary from ×10<sup>-7</sup> to ×10<sup>-9</sup> A/cm<sup>2</sup>. The PSD Ψ<sup>0</sup> values are higher for non-anodized alloys, while in anodized conditions, the values range from -138/-122 dBi (A<sup>2</sup>·Hz<sup>-1</sup>)<sup>1/2</sup> to -131/-180 dBi (A<sup>2</sup>·Hz<sup>-1</sup>)<sup>1/2</sup>. Furthermore, the results indicated that the alloys anodized in the H<sub>3</sub>PO<sub>4</sub> bath showed an electrochemical behavior that can be associated with a more homogeneous passive layer when exposed to the 3.5% wt. NaCl electrolyte. Alloys containing more beta-phase stabilizers formed a less homogeneous anodized layer. These alloys are widely used in aeronautical applications; thus, it is essential that these alloys have excellent corrosion performance in chloride and acid rain environments.

**Keywords:** corrosion; titanium alloys; potentiodynamic polarization; electrochemical noise

## 1. Introduction

The study of oxide films on titanium alloys has recently increased due to its good biological, electrical, and chemical properties [1]. Titanium alloys are widely used in different industries due to their excellent anti-corrosion properties. Titanium alloys can be divided into four categories (α, near-α, α + β, and β). For instance, α titanium and near-α

titanium alloys, such as Ti CP2 and Ti-6Al-2Sn-4Zr-2Mo, respectively, are used in sections of compressor disks, blades, floors, clips, brackets, and in structural zones, whereas  $\alpha+\beta$  alloys (Ti-6Al-4V) are used in landing gear, wings sections, floor support structure, and nacelles. Moreover, the  $\beta$  alloys (Ti Beta-C) are used in frames, ribs, nose landing gear, and actuators [2–4].

However, titanium and titanium alloys may present some corrosion problems under exposure to chloride solutions. When  $\text{Cl}^-$  ions break the passive layer, the accumulation of oxychloride at the metal–film interface provokes the rupture of the oxide film, and a localized corrosion process occurs. In sulfuric acid, the reaction of  $\text{OH}^-$  and  $\text{SO}_4^{2-}$  can create instability of the passive layer. For industries such as aeronautic or aerospace, corrosion can affect the mechanical integrity and safety of affected components, and for the biomedical sector could cause health problems, depending on the alloy used [4–8].

Different surface treatments are used to increase the corrosion resistance of Ti alloys. Techniques such as sol-gel, thermal oxidation, radio frequency magnetron sputtering, electrodeposition, passivation, and anodic oxidation or anodization have been used to obtain a protective oxide layer on the titanium surface [9–11]. The problem with passivation is the low thickness of the coating and the heterogeneity (depending directly on alloying elements) of the oxide layer, i.e., a heterogeneous layer can be prone to localized corrosion. The oxide film accomplished by the sol-gel technique is rich in Ti-OH and it has a thickness lower than  $10\ \mu\text{m}$  [12,13]. Plasma electrolytic oxidation (PEO) is another method that can be very effective, but the requirement of special equipment and the difficulty to process big pieces increase the manufacturing cost. An excellent option to generate oxide layers is anodization. This process can generate a more uniform coating than that obtained by passivation. Moreover, anodization reduces the cost of finished products in comparison to PEO because it can be applied to big pieces [14–16]. The anodization technique is a fast and low-cost technique that allows a more effortless and uniform growth of the passive layer, giving good control of its thickness, composition, and morphology [17–20].

Titanium and its alloys in anodized conditions show better corrosion resistance in atmospheric environments compared to untreated titanium alloys. The surface modification of the alloys through various methods allows new devices to be produced [21–24]. Titanium is a metal reactive to oxygen. The oxidation kinetics occur rapidly and generate a thin layer of  $\text{TiO}_2$  protective against corrosion. The surface condition of Ti alloys will determine the physical and chemical state of the oxide layer. Anodic oxidation or anodization is one of the most used electrochemical methods to generate an oxide layer. This is because it is a fast and inexpensive process. The anodizing process requires an anode (Ti alloys) and a cathode (an inert material, for example, graphite or platinum) immersed in a conductive electrolyte (acid bath). The oxide layer will be formed when an electric current is applied to it, and then the ion diffusion will begin. In various research works, the anodizing process directly depends on the electrolyte, voltage, current, pH, or temperature. These factors can control the uniformity of the oxide layer [25–27].

The galvanostatic anodizing process in electrolytes such as  $\text{H}_2\text{SO}_4$  and  $\text{H}_3\text{PO}_4$  consists of two phases. The anodizing process begins by generating one oxide layer (see phase I in the first few seconds) (Figure 1). Phase II consists of the breakdown of the oxide layer to generate porosities that have an amorphous structure [28].

The passive layer mechanism relates to the ions' diffusion on the surface, in titanium and hydroxyl ions' transfer. When the layer of  $\text{TiO}_2$  is generated, the interface metal–layer–electrolyte will be thermodynamically stable. These conditions increase with oxygen content, and an aqueous media environment facilitates dissociation. Moreover, temperature and pH play an essential role, and if all these factors are correctly combined, a stable oxide layer will be generated [29–34].

Past research [35,36] have demonstrated the titanium behavior in different media and shown that the passive layer generated by the natural process can be weakened due to the diffusion of different ions such as  $\text{Cl}^-$ . A non-uniform passive layer will allow  $\text{Cl}^-$ ,  $\text{Br}^-$ , or  $\text{OH}^-$  ions' diffusion through the oxide layer, increasing the corrosion rate [37,38].

Some works attributed the ions' diffusion through the oxide layer with discontinuities and interstitial penetration [39,40].

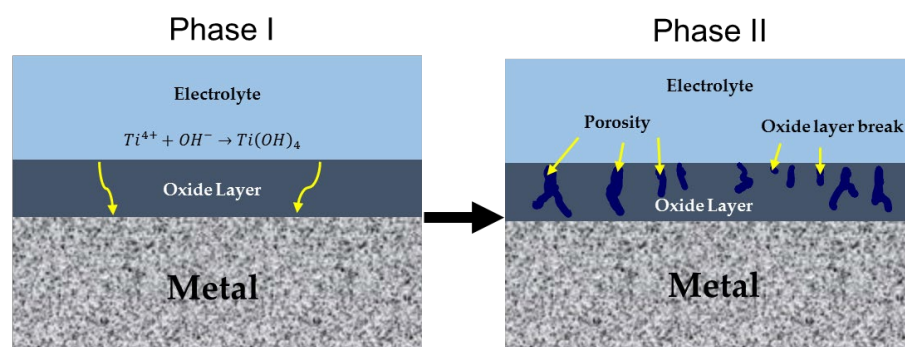


**Figure 1.** Phases of the anodizing process.

Electrochemical techniques are helpful to study the corrosion behavior of this type of material with surface treatments such as anodizing. These techniques allow the analysis of the process and its variables as well as the materials' behavior exposed in different corrosive media. Electrochemical impedance spectroscopy (EIS), electrochemical noise (EN), and potentiodynamic polarization (PP) have been employed by different researchers to determine kinetics and corrosion mechanisms [41–43]. Potentiodynamic polarization technique determines cathodic and anodic reactions, corrosion hysteresis, corrosion rates, and passive layer stability. Attabi et al. [44] indicated the influence of composition and the microstructure of a Ti-6Al-4V alloy on corrosion resistance, and potentiodynamic analysis revealed that icorr decreases using Ti6Al4V-ELI alloys instead of pure titanium in phosphate-buffered solution (PBS). On the other hand, electrochemical impedance spectroscopy (EIS) is used to assess the reaction kinetics of different layers on the surface of the alloys under study. Orazem and Tribollet [45] characterized a Ti-6Al-4V alloy, showing a double-layer structure that increases the corrosion resistance with a surface treatment.

However, techniques such as PP and EIS somehow perturb the corrosion systems through the imposition of an external signal. For this reason, the electrochemical noise (EN) technique is proposed by some authors to analyze material surfaces without perturbation. A particular advantage of EN measurements includes detecting and analyzing the early stages of localized corrosion. Electrochemical noise describes the spontaneous low-level potential and current fluctuations during an electrochemical process. During the corrosion process, predominantly electrochemical cathodic and anodic reactions can cause small transients in electrical charges at the electrode under study.

In addition, EN can be studied by various methods such as time-domain, where analysis is made by visual analysis, skewness, localization index (LI), and noise resistance ( $R_n$ ). Another method to study EN signals is by power spectral density (PSD); this method evaluates frequency signals. Nevertheless, since the EN signal shows different signals (see Equation (1)), it is necessary to separate components that do not apport information about the corrosion process. The DC ( $m_t$ ) component can be separated by different methods, such as the polynomial filter or wavelets. The random ( $S_t$ ) and stationary ( $Y_t$ ) components are considered because the corrosion process occurs in those signals [46–50].

$$x(t) = m_t + s_t + Y_t \quad (1)$$

The separation of the DC signal is necessary because DC creates false frequencies and interferes in visual, statistical, and PSD analysis. The polynomial method is governed by Equation (2), where  $x_n$  is the EN signal with all the components, a polynomial of “ $n$ ” grade

( $p_0$ ) at  $n$ -th term ( $a_i$ ) in “ $n$ ” time to obtain a signal without trend ( $y_n$ ) [51,52]. In this work, a 9th-degree polynomial was applied.

$$y_n = x_n - \sum_{i=0}^{p_0} a_i n^i \quad (2)$$

In order to perform PSD, analysis is necessary to transform the time-domain to a frequency domain signal. Usually, fast Fourier transform (FFT) is used to process the EN signal. Equations (3) and (4) show how to calculate the spectral density [53].

$$R_{xx}(m) = \frac{1}{N} \sum_{n=0}^{N-m-1} x(n) \times x(n+m), \quad \text{when values are from } 0 < m < N \quad (3)$$

$$\Psi_x(k) = \frac{\gamma \times t_m}{N} \times \sum_{n=1}^N (x_n - \bar{x}_n) \times e^{-\frac{2\pi kn^2}{N}} \quad (4)$$

Another advantageous method to determine the type of corrosion is wavelets. The wavelets method does not need the application of a polynomial filter because decomposition of the EN signal separates DC from the corrosion signal. The decomposition is by a high–low filter, high frequencies are named detail (D), and low are called approximation (S). Equation (5) gives the way to obtain the total energy for a system of  $N$  data number [5,54]

$$E = \sum_{n=1}^N x_n^2 \quad (5)$$

The energy fraction presented in detail and approximation is given by Equation (6).

$$ED_j^d = \frac{1}{E} \sum_{n=1}^N d_{j,n}^2 \quad ED_j^s = \frac{1}{E} \sum_{n=1}^N s_{j,n}^2 \quad (6)$$

The accumulation of energy will determine the process occurring on the surface. High energy in crystals from D1 to D3 is related to metastable pitting. Crystals from D4 to D6 are related to localized corrosion, and crystals from D7 to D8 are related to long process corrosion (diffusion or general corrosion) [36,37].

This work aimed to study the electrochemical behavior of anodizing on Ti CP2 and alloys Ti-6Al-2Sn-4Zr-2Mo, Ti-6Al-4V, and Ti Beta-C immersed in 3.5% wt. NaCl and H<sub>2</sub>SO<sub>4</sub> solutions at room temperature. The electrochemical behavior was studied by cyclic potentiodynamic polarization and electrochemical noise, and the characterization of the titanium oxide layer was conducted using scanning electron microscopy (SEM). Titanium alloys are used in various aircraft components and exposed to different marine and industrial (acid rain) atmospheres. Exposure in marine environments implies the presence of chlorides as the main corrosive agent. In an industrial environment, sulfuric acid can simulate an acid rain environment, which is formed from the chemical reactions of sulfur dioxide and nitrogen oxides found in the atmosphere with water and chemical contaminants resulting in nitric sulfuric acids.

## 2. Materials and Methods

### 2.1. Material

The materials used in this work were Ti CP2 and alloys: Ti-6Al-2Sn-4Zr-2Mo, Ti-6Al-4V, and Ti Beta-C, tested in the as-received state. The chemical composition of these alloys was obtained by atomic absorption spectrometry, Table 1.

**Table 1.** Chemical Composition of the Ti CP2 and its alloys (% wt.).

Elements	Ti CP2	Alloys		
		Ti-6Al-2Sn-4Zr-2Mo	Ti-6Al-4V	Ti Beta-C
Fe	0.038 ± 0.005	–	0.21 ± 0.01	0.08 ± 0.01
Al	–	6.75 ± 0.20	7.14 ± 0.37	4.2 ± 0.13
V	–	–	4.03 ± 0.08	8.1 ± 0.07
Zr	–	4.18 ± 0.01	–	4.3 ± 0.01
Cr	–	–	–	3.3 ± 0.07
Mo	–	1.99 ± 0.008	–	3.9 ± 0.01
Sn	–	2.08 ± 0.01	–	–
Ti	99.94 ± 0.005	84.65 ± 0.19	87.71 ± 0.36	75.2 ± 0.14

## 2.2. Microstructural Characterization

Titanium samples were prepared by the metallography technique [54]. The various alloys were ground using 400, 600, and 800 grade SiC sandpaper followed by ultrasonic cleaning in ethanol (C<sub>2</sub>H<sub>5</sub>OH) and deionized water for 10 min for each sample. The chemical attack of the samples was carried out using Kroll solution composed of 3 mL of HF, 5 mL of HNO<sub>3</sub>, and 100 mL of water [55].

The surface morphology was investigated using a scanning electron microscope ((SEM) JEOL-JSM-5610LV, Tokyo, Japan) operating at 20 kV and 12 and 8.5 mm working distance. The surface micrographs by SEM were taken using backscattered electron (BSE) and secondary electron (SE) detectors. The porosity percentage analysis was carried out by optical microscopy (OM, Carl Zeiss Microscopy GmbH, Jena, Germany).

## 2.3. Anodizing Process

Pretreatment consisted of ultrasonic cleaning in ethanol (C<sub>2</sub>H<sub>5</sub>OH) and deionized water. The anodizing process was carried out in an electrochemical cell with a graphite rod as cathode and a 1 M sulfuric (H<sub>2</sub>SO<sub>4</sub>) and phosphoric acid (H<sub>3</sub>PO<sub>4</sub>) electrolytes (analytical grade reagents (J.T. Baker)) at 25 ± 1 °C. The current density of the titanium samples was 0.025 A·cm<sup>-2</sup> for 600 s using a DC power supply (XLN300025-GL). The anodizing process was carried out under the specification AMS2487 [56].

## 2.4. Electrochemical Measurements

Cyclic potentiodynamic polarization (CPP) and electrochemical noise (EN) measurements were conducted at room temperature using a Gill-AC potentiostat/galvanostat/ZRA (Zero Resistance Ammeter) from ACM Instruments (Manchester, UK) in 3.5% wt. NaCl and H<sub>2</sub>SO<sub>4</sub> solutions, with the latter reagent used to simulate acid rain conditions. A conventional three-electrode cell configuration was used for electrochemical corrosion studies, which consisted of a working electrode, WE (Titanium and its alloys), a reference electrode, RE (saturated calomel electrode (SCE)), and a counter electrode, CE (platinum mesh) [57,58]. Corrosion tests were realized in triplicate.

The CPP measurements were conducted over a potential scan range between –1.2 and 1.2 V vs. SCE from corrosion potential (E<sub>corr</sub>), using a scan rate of 1 mV/sec [59–61].

A digital sampling performed electrochemical noise (EN) measurements of current and potential values at one-second intervals on the specimens tested. The time records consisted of 4096 data. The electrochemical cell for EN measurements consisted of anodized titanium samples (working electrode WE1), a platinum electrode (WE2), and a saturated calomel electrode as reference electrode (RE). EN data was processed with a program made in MATLAB 2018a software (Math Works, Natick, MA, USA). It removes the trends with a polynomial grade 9 and fast Fourier transform (FFT) with a Hann windowing [36,37,62–66].

### 3. Results and Discussion

#### 3.1. SEM Microstructural Analysis

The superficial morphology of the anodized titanium and titanium alloy samples was analyzed by SEM.

Figure 2a shows an SEM surface micrograph using a backscattered electron (BSE) detector for Ti CP2, where an  $\alpha$ -phase microstructure matrix with large grain size is observed. Figure 2b shows the Ti-6Al-4V microstructure is fine and equiaxed because the cooling was slow in the recrystallization alloy. The  $\alpha$  and  $\beta$  phases are marked with blue arrows. This phase has spherical shapes and  $\alpha$  phases. The  $\beta$  phase increases in Ti-6Al-4V due to elements such as vanadium retained in  $\beta$ , so if vanadium or molybdenum increases its concentration in Ti alloys, the  $\beta$  phase will increase. Figure 2c shows the surface microstructure of Ti-6Al-2Sn-4Zr-2Mo; the alloy has grains of  $\alpha$  phase, with an appreciable deformation and angular shapes located at triple points and corresponding to the  $\beta$  phase. Figure 2d shows a  $\beta$ -phase microstructure matrix for the Ti Beta-C alloy. For Ti CP2, Ti-6Al-2Sn-4Zr-2Mo, and Ti-6Al-4V alloys, porosity from the manufacturing process (about 1 to 2  $\mu\text{m}$  in diameter) was observed.

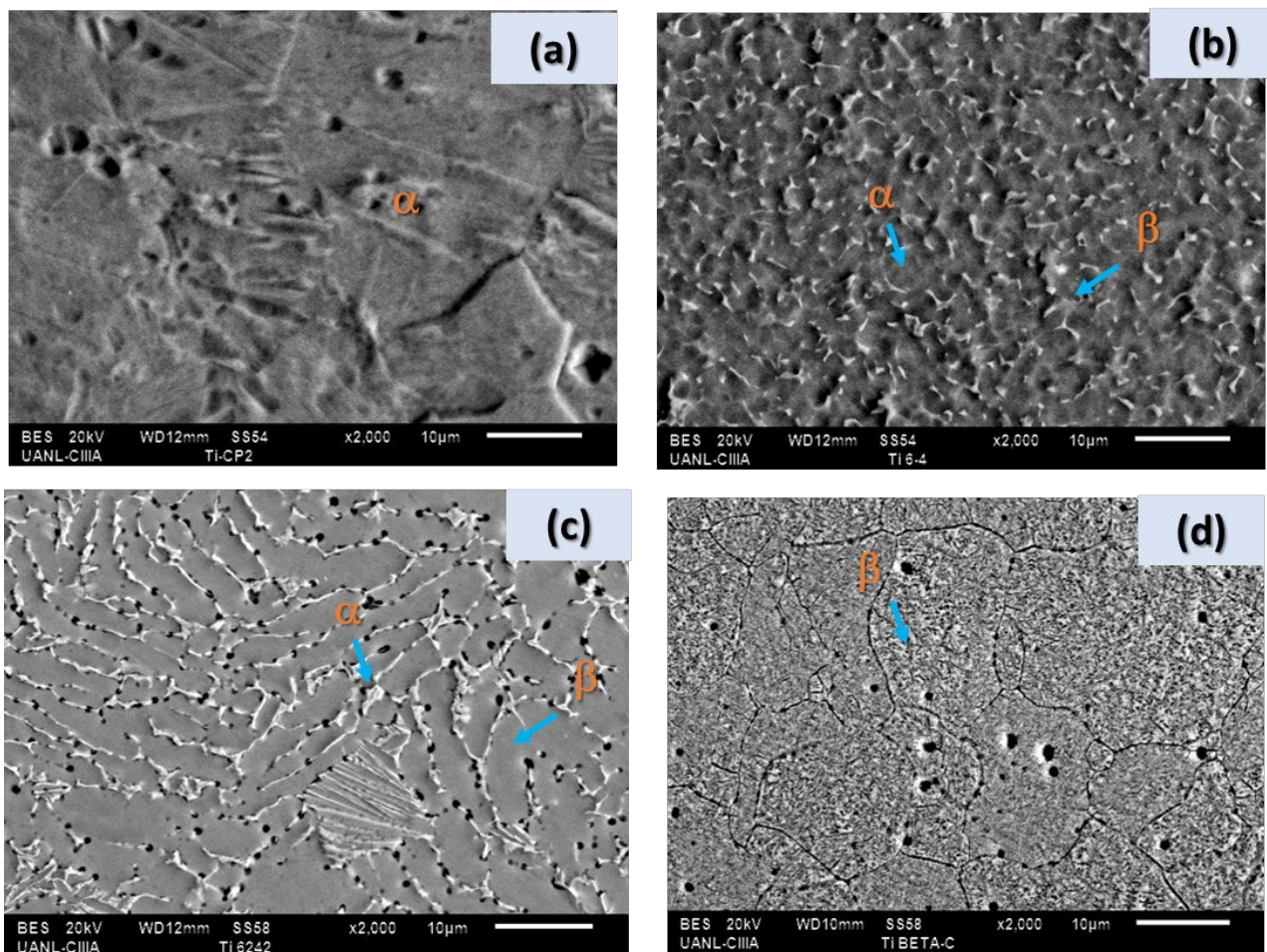


**Figure 2.** SEM–BSE surface micrographs of titanium and alloys (initial conditions): (a) CP2 (b) Ti-6Al-4V (c) Ti-6Al-2Sn-4Zr-2Mo (d) Ti Beta-C.

#### 3.2. SEM–OM Surface Analysis of Anodized Alloys

Figure 3 shows the surface micrographs by SEM using a secondary electron (SE) detector for anodized samples anodized in an  $\text{H}_2\text{SO}_4$  bath. Anodized Ti CP2 and Ti-6Al-2Sn-4Zr-2Mo presented a homogenous porosity distribution. However, anodized Ti-6Al-2Sn-4Zr-2Mo has a smaller porosity than Ti CP2. For Ti-6Al-4V, porosity is homogenous

but smaller. Ti Beta-C presents porosity and superficial cracking. All the samples anodized in  $H_2SO_4$  presented a homogenous porosity distribution. In order to evaluate the porosity percent in the samples, these were analyzed by optical microscopy (OM) using ZEN Image analysis software—multiphase module. The obtained results were: Ti CP2 (12.5%), Ti-6Al-2Sn-4Zr-2Mo (11.3%), Ti-6Al-4V (13.1%), and Ti Beta-C (8.6%). These values are for samples anodized in  $H_2SO_4$ .

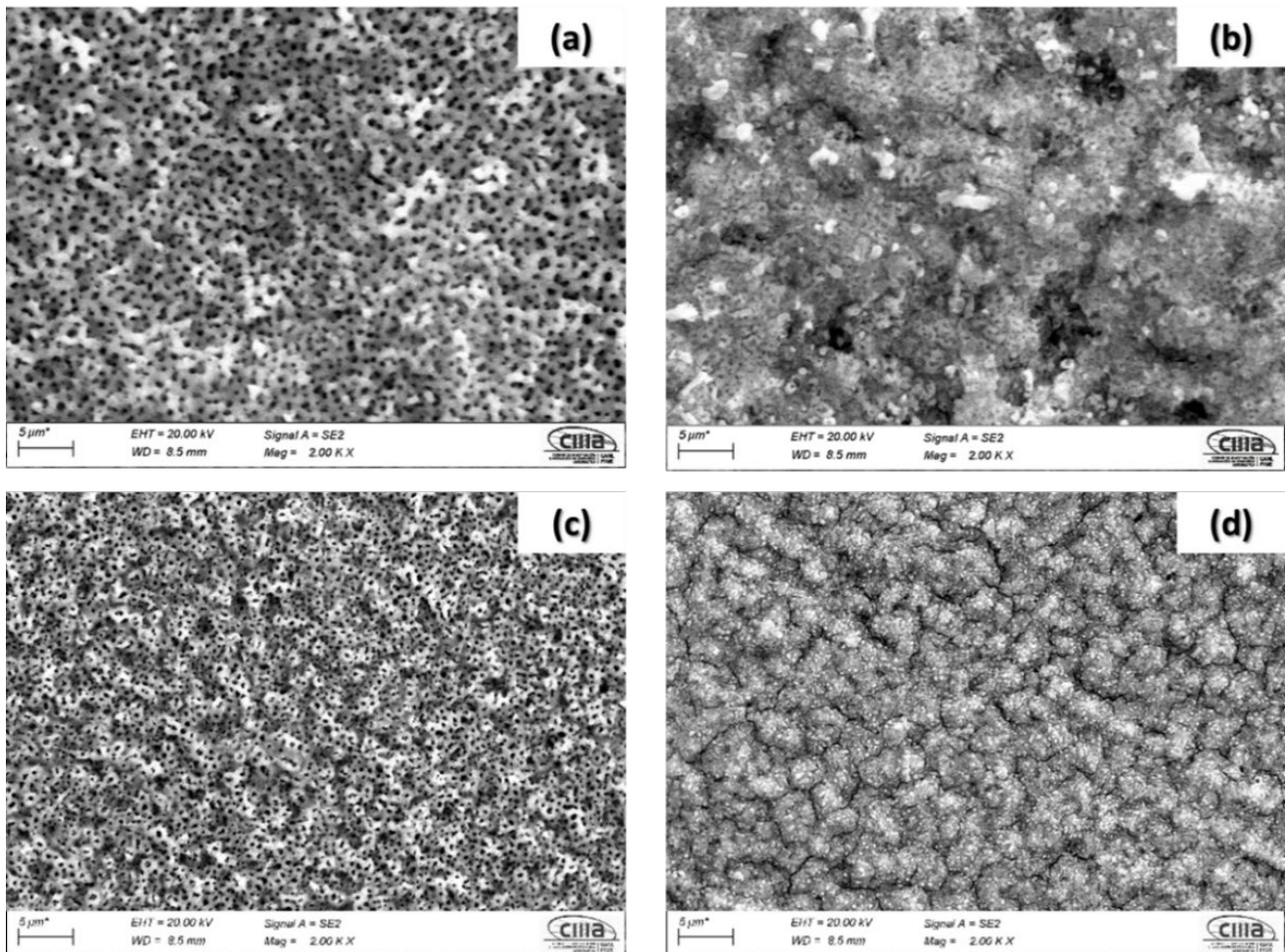


**Figure 3.** SEM–SE surface micrographs of anodized titanium and alloy samples in  $H_2SO_4$  bath at  $2000\times$ . (a) Ti CP2 (b) Ti-6Al-4V (c) Ti-6Al-2Sn-4Zr-2Mo and (d) Ti Beta-C.

Figure 4 shows the SEM surface micrographs using secondary electrons (SE) of samples anodized in  $H_3PO_4$ . Compared to samples anodized in  $H_2SO_4$ , these anodized samples present less porosity, which is not distributed in a homogeneous way, and they also present larger porosities. All the samples presented microporosity on the surface; the anodized Ti Beta-C (Figure 4d) has smaller porosity, and this morphology may help to increase the corrosion resistance. Anodized Ti-6Al-2Sn-4Zr-2Mo and Ti-6Al-4V samples presented a similar morphology. Ti Beta-C (Figure 4d) anodized in  $H_3PO_4$  show similar features to that anodized in an  $H_2SO_4$  bath (Figure 3d), with smaller porosity and surface cracking; however, this does not necessarily indicate a low corrosion resistance as the cracks may only be on the surface. The porosity percentages of the anodized samples in the  $H_3PO_4$  bath were as follows 13.2%, 19.77%, 14.6%, and 7.0% for Ti CP2, Ti-6Al-2Sn-4Zr-2Mo, Ti-6Al-4V, and Ti Beta-C, respectively.

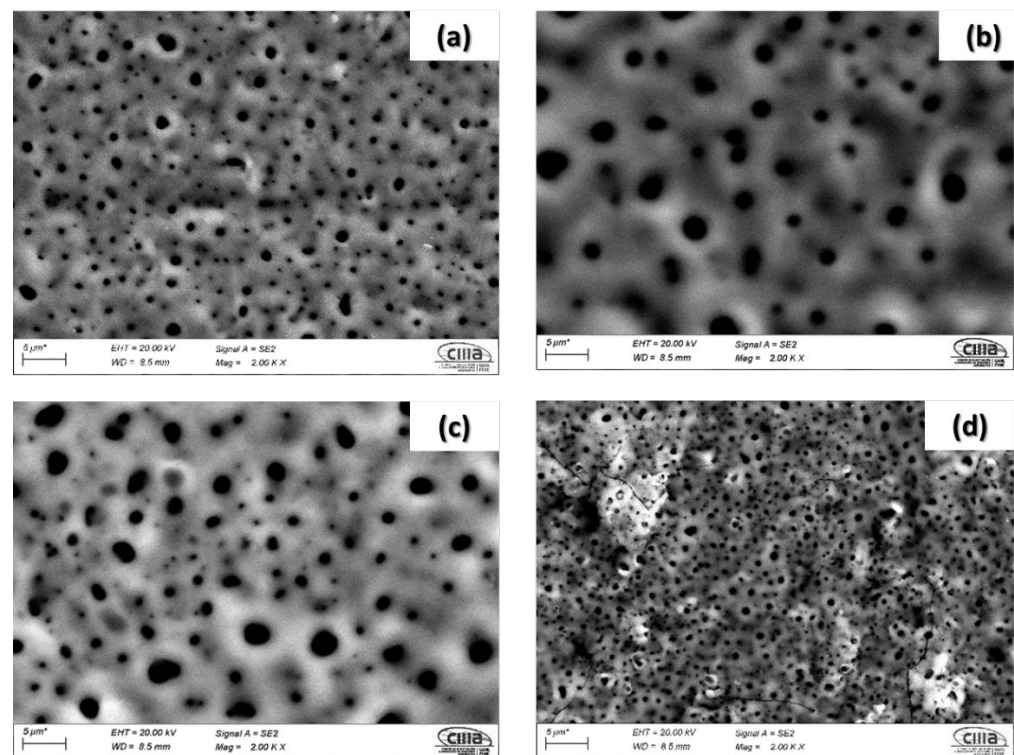


**Figure 4.** SEM-SE surface micrographs of anodized titanium and alloy samples in  $H_3PO_4$  bath at  $2000\times$ . (a) Ti CP2, (b) Ti-6Al-4V, (c) Ti-6Al-2Sn-4Zr-2Mo, and (d) Ti Beta-C.

### 3.3. Cyclic Potentiodynamic Polarization (CPP)

The corrosion kinetic behavior of anodized titanium and alloys using cyclic potentiodynamic polarization can be studied through cathodic and anodic reactions under exposure to 3.5% wt. NaCl and  $H_2SO_4$  solutions (see Figures 5 and 6).

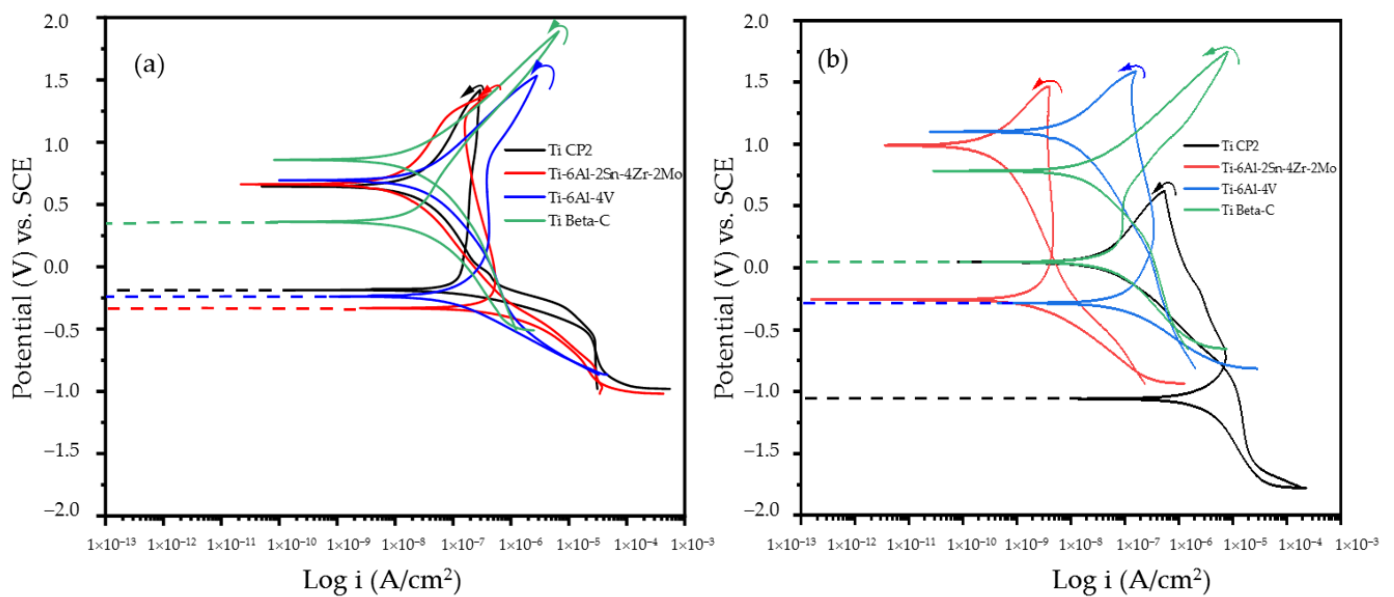


**Figure 5.** Cyclic potentiodynamic polarization of anodized titanium and alloy samples in (a)  $H_2SO_4$  bath and (b)  $H_3PO_4$  bath immersed in 3.5% wt. NaCl solution.

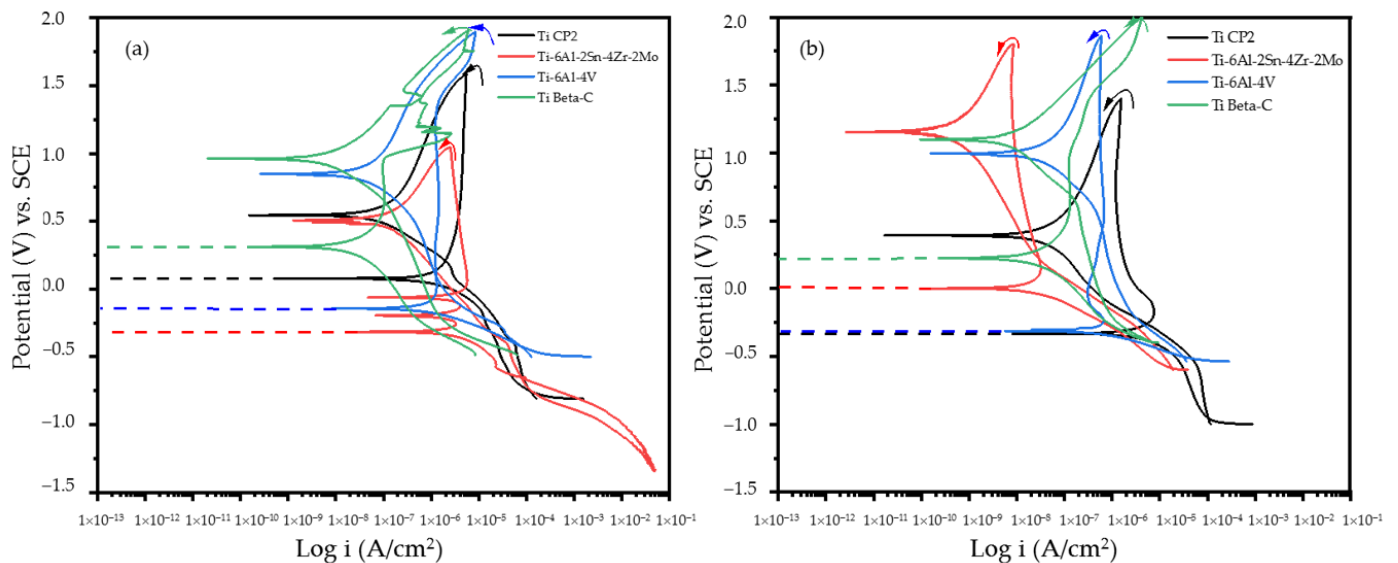


**Figure 6.** Cyclic potentiodynamic polarization of anodized titanium and alloy samples in (a)  $\text{H}_2\text{SO}_4$  bath and (b)  $\text{H}_3\text{PO}_4$  bath immersed in 3.5% wt.  $\text{H}_2\text{SO}_4$  solution.

Figure 5 shows the results of CPP in NaCl 3.5% wt. for samples anodized in (a)  $\text{H}_2\text{SO}_4$  and (b)  $\text{H}_3\text{PO}_4$ . In Figure 5a, all samples presented uniform corrosion (negative hysteresis). Ti-6Al-2Sn-4Zr-2Mo alloy showed the lower  $E_{\text{corr}}$  ( $-0.33$  V), whereas Ti Beta-C showed a higher  $E_{\text{corr}}$  ( $0.15$  V) value. These results can be related to a more active  $E_{\text{corr}}$  behavior of the anodized Ti-6Al-2Sn-4Zr-2Mo.

Further,  $i_{\text{corr}}$  values of all samples are related to  $E_{\text{corr}}$ , with Ti Beta-C presenting the lowest  $i_{\text{corr}}$  ( $9.12 \times 10^{-9}$  A/cm $^2$ ), which is associated with lower corrosion kinetics. However, the anodized Ti Beta-C was the only one that did not present a passive behavior; this could be attributed to the dissolution of the anodized solution in this media. Moreover, titanium with alloying elements presented passive layer breakdown. Figure 5b presents a similar behavior for Ti Beta-C; however, in the media presented, a passivation range can be noted, where the passive layer prevents the material dissolution. Ti CP2 and Ti-6Al-4V showed a decrease in current demand in the passive zone, and this is related to the addition of ions to the surface, decreasing the electrons' transfer.

Figure 6 shows the results of CPP in  $\text{H}_2\text{SO}_4$  3.5% wt. for samples anodized in (a)  $\text{H}_2\text{SO}_4$  and (b)  $\text{H}_3\text{PO}_4$ . The  $E_{\text{corr}}$  behavior presented in Figure 6a,b is very similar to that in Figure 5a,b. Figure 6a shows that the anodized Ti-6Al-2Sn-4Zr-2Mo presented the lower  $E_{\text{corr}}$  ( $-0.31$  V) and higher  $i_{\text{corr}}$  ( $1.16 \times 10^{-5}$  A/cm $^2$ ) values. On the other hand, Ti Beta-C presents the higher  $E_{\text{corr}}$  ( $0.31$  V) and the lower  $i_{\text{corr}}$  ( $4.1 \times 10^{-8}$  A/cm $^2$ ). However, the anodized Ti Beta-C showed a passive range ( $0.35$  V), indicating that anodization prevents ions' penetration, with the activation process after passivation being more aggressive, and transpassivation is unstable. Additionally, anodized Ti-6Al-2Sn-4Zr-2Mo presents multiple reactions in the anodic branch. This behavior is related to  $\text{OH}^-$  ions' reaction and a more unstable passive layer. All samples presented negative hysteresis related to a general corrosion process (see Table 2). It is important to mention that anodizing with more beta stabilizers has a similar behavior, Ti-6Al-4V relates to Ti Beta-C and Ti-6Al-2Sn-4Zr-2Mo with Ti CP2. Figure 6b shows the results of anodizing with  $\text{H}_3\text{PO}_4$ , where Ti Beta-C presents the higher  $E_{\text{corr}}$  with the lower  $i_{\text{corr}}$  values. Anodized Ti CP2 and Ti-6Al-2Sn-4Zr-2Mo showed a decrease in current demand in the passive zone, related to the adsorption of ions in the surface at these potentials.

**Table 2.** Electrochemical parameters obtained from CPP.

Alloy	$E_{\text{corr}}$ (V)	$i_{\text{corr}}$ (A/cm <sup>2</sup> )	Active–Passive Trans (V)	Hysteresis	Range Passive (V)	Passive Breakdown (V)
Titanium and alloys anodized in H <sub>2</sub> SO <sub>4</sub>						
3.5% wt. NaCl						
Ti CP2	0.19	$1.04 \times 10^{-7}$	–	Negative	0.85	0.83
Ti-6Al-2Sn-4Zr-2Mo	−0.33	$3.07 \times 10^{-7}$	–	Negative	1.29	1.19
Ti-6Al-4V	−0.24	$6.65 \times 10^{-8}$	–	Negative	0.48	0.77
Ti Beta-C	0.15	$9.12 \times 10^{-9}$	–	Negative	–	–
3.5% wt. H <sub>2</sub> SO <sub>4</sub>						
Ti CP2	0.07	$7.98 \times 10^{-7}$	–	Negative	0.94	1.53
Ti-6Al-2Sn-4Zr-2Mo	−0.31	$1.16 \times 10^{-5}$	–	Negative	0.96	1.02
Ti-6Al-4V	−0.14	$1.69 \times 10^{-6}$	–	Negative	1.27	1.28
Ti Beta-C	0.31	$4.1 \times 10^{-8}$	–	Negative	0.35	0.96
Titanium and alloys anodized in H <sub>3</sub> PO <sub>4</sub>						
3.5% wt. NaCl						
Ti CP2	−1.05	$1.06 \times 10^{-7}$	–	Negative	1.26	0.59
Ti-6Al-2Sn-4Zr-2Mo	−0.25	$5.09 \times 10^{-7}$	–	Negative	1.24	1.42
Ti-6Al-4V	−0.28	$4.24 \times 10^{-7}$	–	Negative	1.17	1.44
Ti Beta-C	0.05	$2.24 \times 10^{-8}$	–	Negative	0.20	0.48
3.5% wt. H <sub>2</sub> SO <sub>4</sub>						
Ti CP2	−0.34	$3.43 \times 10^{-8}$	–	Negative	1.42	1.28
Ti-6Al-2Sn-4Zr-2Mo	0.01	$3.24 \times 10^{-8}$	–	Negative	1.6	1.75
Ti-6Al-4V	−0.31	$4.60 \times 10^{-7}$	–	Negative	1.25	1.78
Ti Beta-C	0.22	$3.1 \times 10^{-8}$	–	Negative	0.37	0.94

### 3.4. Electrochemical Noise

#### 3.4.1. PSD Analysis

The electrochemical noise technique was evaluated by the PSD and wavelets methods. Using a polynomial grade 9th filter, PSD was made to remove the DC signal. For PSD analysis, it is necessary to transform from the time-domain to the frequency domain applying an FFT. The interpretation of PSD will depend on the slope or change in the slope behavior. The frequency zero limits ( $\psi^0$ ) result in material dissolution [64–66]. Table 3 (adapted to decibels) associates slope values with the corrosion type, and Equation (7) explains how to obtain the slope value. It is important to point out that some values are the same for two types of corrosion; this could lead to another way of studying the slope and frequencies [66–70].

$$\log \Psi_x = -\beta_x \log f \quad (7)$$

**Table 3.**  $\beta$  intervals to indicate the type of corrosion [63].

Corrosion Type	dB(V)·Decade <sup>−1</sup>		dB(A)·Decade <sup>−1</sup>	
	Minimum	Maximum	Minimum	Maximum
Uniform	0	−7	0	−7
Pitting	−20	−25	−7	−14
Passive	−15	−25	−1	1

Figure 7 shows the PSD in voltage (a, c) and current (b, d) for samples anodized in H<sub>2</sub>SO<sub>4</sub> and H<sub>3</sub>PO<sub>4</sub>, respectively, exposed in 3.5% wt. NaCl. Figure 7a presents the behavior of anodized samples Ti-6Al-4V and Ti Beta-C showing a similar behavior without significant potential variations in frequencies, meaning that the process did not change and only occurs once (uniform process). Ti-6Al-2Sn-4Zr-2Mo presents a lower slope value

(−8.8), see Table 3. This could mean a non-homogenous anodizing (porosities). The PSD in current for anodized samples in 3.5% wt.  $H_2SO_4$  solution presents changes in the slope. This behavior is related to changes in the corrosion process or diverse reactions in the anodized surface due to appreciable porosity. Moreover, Ti CP2 presented the higher value of  $\Psi^0$  (−131.48 dBi), associated with higher corrosion kinetics.

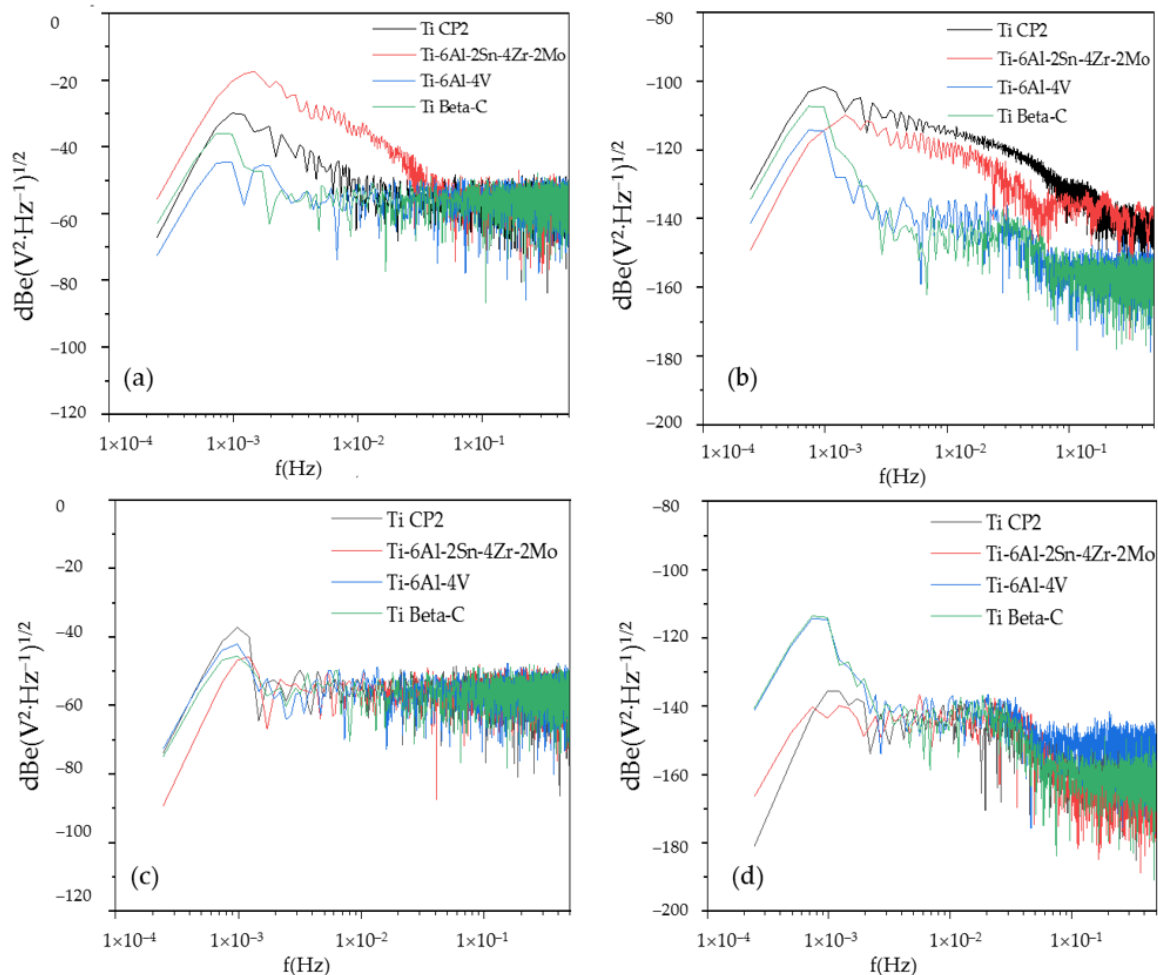


**Figure 7.** Power spectral density (PSD) in voltage for anodized titanium and alloy samples in (a)  $H_2SO_4$  and (c)  $H_3PO_4$ . In current for (b)  $H_2SO_4$  and (d)  $H_3PO_4$  immersed in 3.5% wt. NaCl solution.

Figure 7c shows the behavior of samples anodized in an  $H_3PO_4$  solution. All samples showed slope values indicative of uniform corrosion, and this was associated with an ion transference balance. In Figure 4d,  $\Psi^0$  is higher for Ti Beta-C. Here, a higher corrosion kinetic can be related to the dissolution of a stable passive layer. Meanwhile, anodized Ti CP2 showed a higher corrosion resistance. Anodized Ti-6Al-2Sn-4Zr-2Mo and Ti Beta-C shows a slope associated with pitting corrosion (see Table 3); this behavior should be associated with the presence of porosities in the anodized layer.

Figure 8 shows the PSD in voltage (a, c) and current (b, d) for  $H_2SO_4$  and  $H_3PO_4$ , respectively, immersed in 3.5% wt  $H_2SO_4$  solution. Figure 8a,c presents a similar behavior, with slope values corresponding to uniform corrosion (see Table 3), meaning a stable ions transfer in an anodized surface. Figure 8b shows the PSD in current. Here, anodized Ti-6Al-4V presents a higher dissolution (−135 dBi). On the other hand, Ti Beta-C showed the lower dissolution (−154 dBi). The slope values change in frequencies, indicating a non-uniform current distribution in the material surface, and this could be related to a non-uniform anodizing.

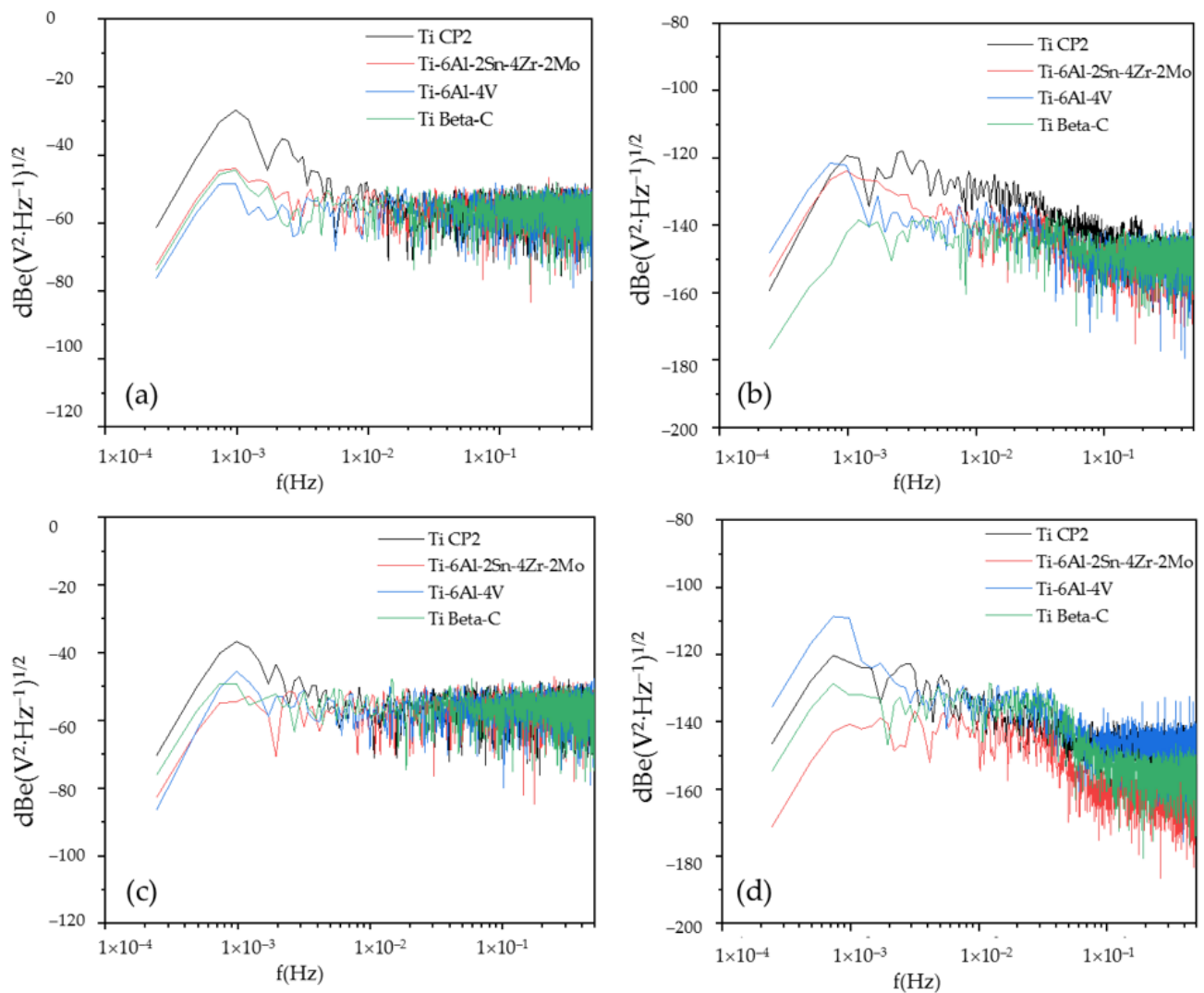


**Figure 8.** Power spectral density (PSD) in voltage for anodized titanium and alloy anodized samples in (a)  $\text{H}_2\text{SO}_4$  and (c)  $\text{H}_3\text{PO}_4$ . In current for (b)  $\text{H}_2\text{SO}_4$  and (d)  $\text{H}_3\text{PO}_4$  immersed in 3.5% wt.  $\text{H}_2\text{SO}_4$  solution.

The noise impedance ( $Z_n$ ), also called spectral noise resistance, is expressed by the following equation [50,61,71]

$$Z_n = \sqrt{\frac{\psi_V(f)}{\psi_I(f)}} \quad (8)$$

$Z_n$  is calculated by the PSD of potential and current division square root. The electrochemical noise impedance zero ( $Z_{n0}$ ) is related to corrosion resistance [47,69].

Figure 9 shows the noise impedance ( $Z_n$ ), which is homologous to noise resistance ( $R_n$ ). The Ti-6Al-2Sn-4Zr-2Mo anodized in  $\text{H}_2\text{SO}_4$  and  $\text{H}_3\text{PO}_4$  immersed in NaCl and  $\text{H}_2\text{SO}_4$  solutions showed the higher resistance in both media (see  $Z_{n0}$  in Table 4). All the samples, except the Ti-6Al-2Sn-4Zr-2Mo, anodized in  $\text{H}_2\text{SO}_4$  and exposed in 3.5% wt. NaCl, show an increase in the slope, so  $Z_n$  increases at high frequencies. This may indicate that a fast process does not affect the corrosion resistance.

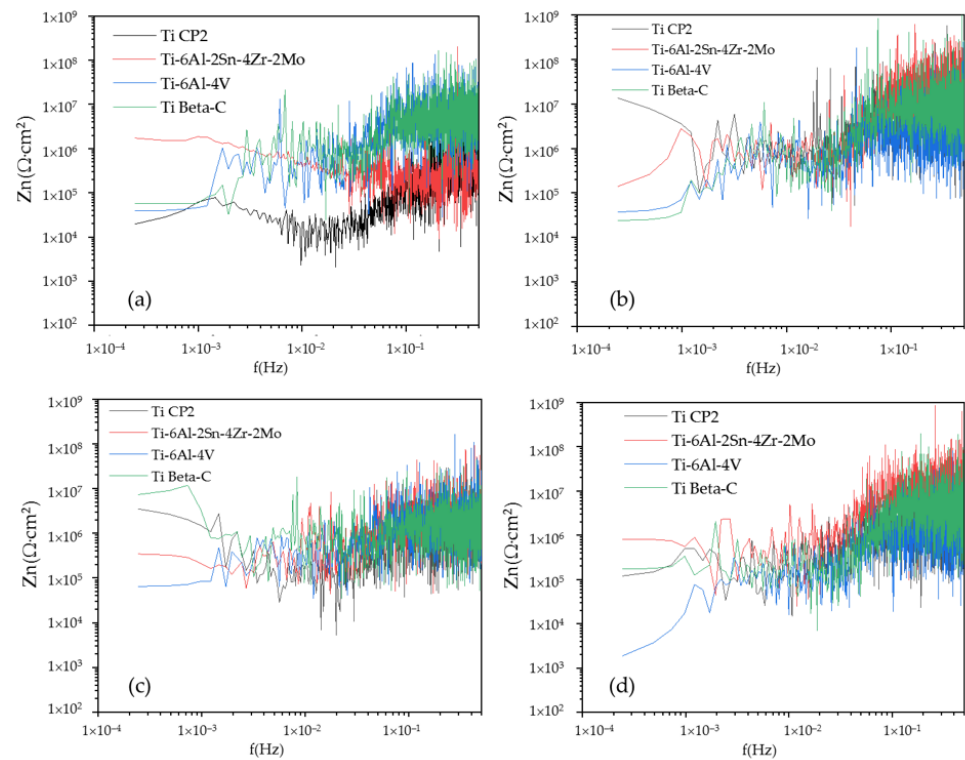


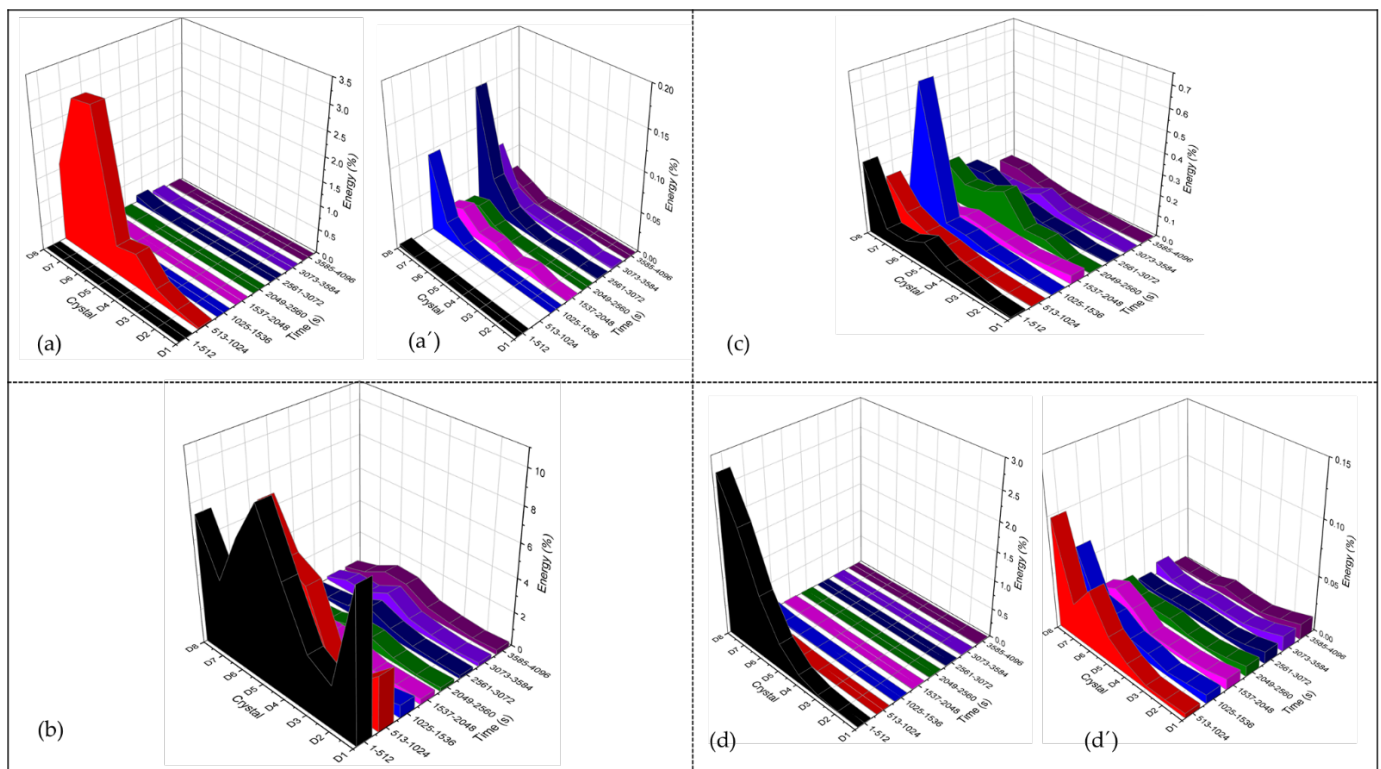
**Figure 9.** Noise impedance ( $Z_n$ ) for anodized titanium and alloys samples in (a)  $H_2SO_4$  and (b)  $H_3PO_4$  in NaCl at 3.5% wt. (c)  $H_2SO_4$  and (d)  $H_3PO_4$  immersed in 3.5% wt.  $H_2SO_4$  solution.

**Table 4.** Parameters obtained by PSD.

Titanium and Alloys Anodized in $H_2SO_4$				
3.5% wt. NaCl				
Alloys	$\Psi^0$ (dBi)	B (dB (V))	B (dB (A))	$Z_{n0}$ ( $\Omega \cdot cm^2$ )
Ti CP2	−131.48	−2.13	−16.34	$19.46 \times 10^3$
Ti-6Al-2Sn-4Zr-2Mo	−149.19	−8.50	−9.00	$17.29 \times 10^5$
Ti-6Al-4V	−141.30	−0.10	−8.36	$38.75 \times 10^3$
Ti Beta-C	−134.42	−0.20	−8.88	$57.80 \times 10^3$
3.5% wt. $H_2SO_4$				
Ti CP2	−159.42	−1.15	−10.02	$34.94 \times 10^5$
Ti-6Al-2Sn-4Zr-2Mo	−155.25	0.08	−6.38	$34.37 \times 10^4$
Ti-6Al-4V	−148.33	0.44	−5.12	$64.72 \times 10^3$
Ti Beta-C	−176.70	0.07	−2.59	$72.97 \times 10^5$
Titanium and Alloys Anodized in $H_3PO_4$				
3.5% wt. NaCl				
Alloys	$\Psi^0$ (dBi)	B (dB (V))	B (dB (A))	$Z_{n0}$ ( $\Omega \cdot cm^2$ )
Ti CP2	−180.98	−0.47	−6.84	$13.63 \times 10^6$
Ti-6Al-2Sn-4Zr-2Mo	−166.41	0.71	−13.77	$13.89 \times 10^4$
Ti-6Al-4V	−141.21	0.08	−5.74	$36.98 \times 10^3$
Ti Beta-C	−140.51	0.39	−9.97	$23.68 \times 10^3$
3.5% wt. $H_2SO_4$				
Ti CP2	−146.53	−0.08	−5.63	$12.03 \times 10^4$
Ti-6Al-2Sn-4Zr-2Mo	−171.24	0.99	−9.53	$79.92 \times 10^4$
Ti-6Al-4V	−135.63	1.11	−7.04	$18.77 \times 10^2$
Ti Beta-C	−154.68	0.15	−12.00	$17.24 \times 10^4$

### 3.4.2. Wavelets Analysis

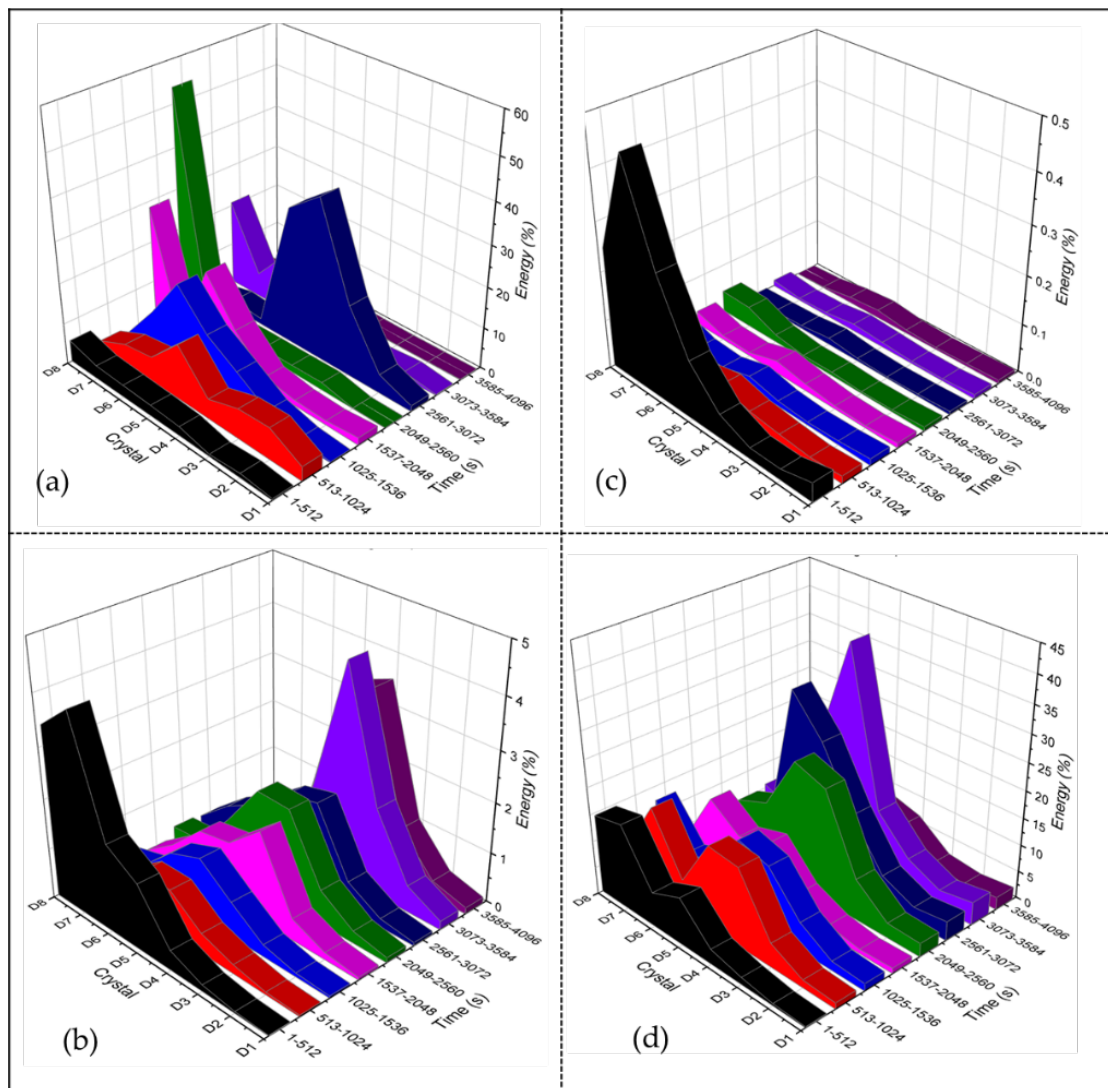
Figure 10 shows the wavelets analysis for Ti CP2 anodized in  $H_2SO_4$  and  $H_3PO_4$  and exposed to NaCl and  $H_2SO_4$ . Figure 10a presents the result for the  $H_2SO_4$  anodizing exposed in 3.5% wt. NaCl, indicating that energy accumulates in low-frequency crystals. The time from 1–512 and 512–1024 s in the last crystal are related to a uniform porosity at the surface. First time-lapses of 1–512 and 513–1024 (black and red graphics) give the material surface (porosity) information. After removing the time-lapse 513 to 1024 s to make a windowing of wavelets analysis, Figure 10a' shows the behavior of the long time-lapse. Long-time crystals reflect the corrosion conduct after thermodynamic stabilization of the material–electrolyte interface. For Figure 10a', crystals D7 and D8 present higher energy accumulation, related to the diffusion of ions of  $Cl^-$  on the surface. Figure 10b shows the same anodized exposure on  $H_2SO_4$ . For this case, the energy is distributed in the middle crystals; the behavior is associated with  $H^-$  and  $OH^-$  presence. Those ions are smaller than  $Cl^-$ , so they are probably porous. Figure 10c shows a high accumulation of energy in crystal D6, this for non-uniform distribution of porosities. On the other hand, Figure 10d shows high energy accumulation for the last crystals of lapse 1–512 s. In Figure 10d', the behavior presented is commonly from a passivated system with energy distributed equitably in all crystals in time-lapses of 2049 to 4096 s.



**Figure 10.** Wavelets analysis for Ti CP2 anodized immersed in 3.5% wt. NaCl and  $H_2SO_4$  solutions. (a,c)  $H_2SO_4$  bath, (b,d)  $H_3PO_4$  bath, and (a',d') windowing of wavelets analysis.

Figure 10c shows a high accumulation of energy in crystal D6, this for non-uniform distribution of porosities. On the other hand, Figure 10d shows high energy accumulation for the last crystals of lapse 1–512 s. In Figure 10d', the behavior presented is commonly from a passivated system with energy distributed equitably in all crystals in time-lapses of 2049 to 4096 s.

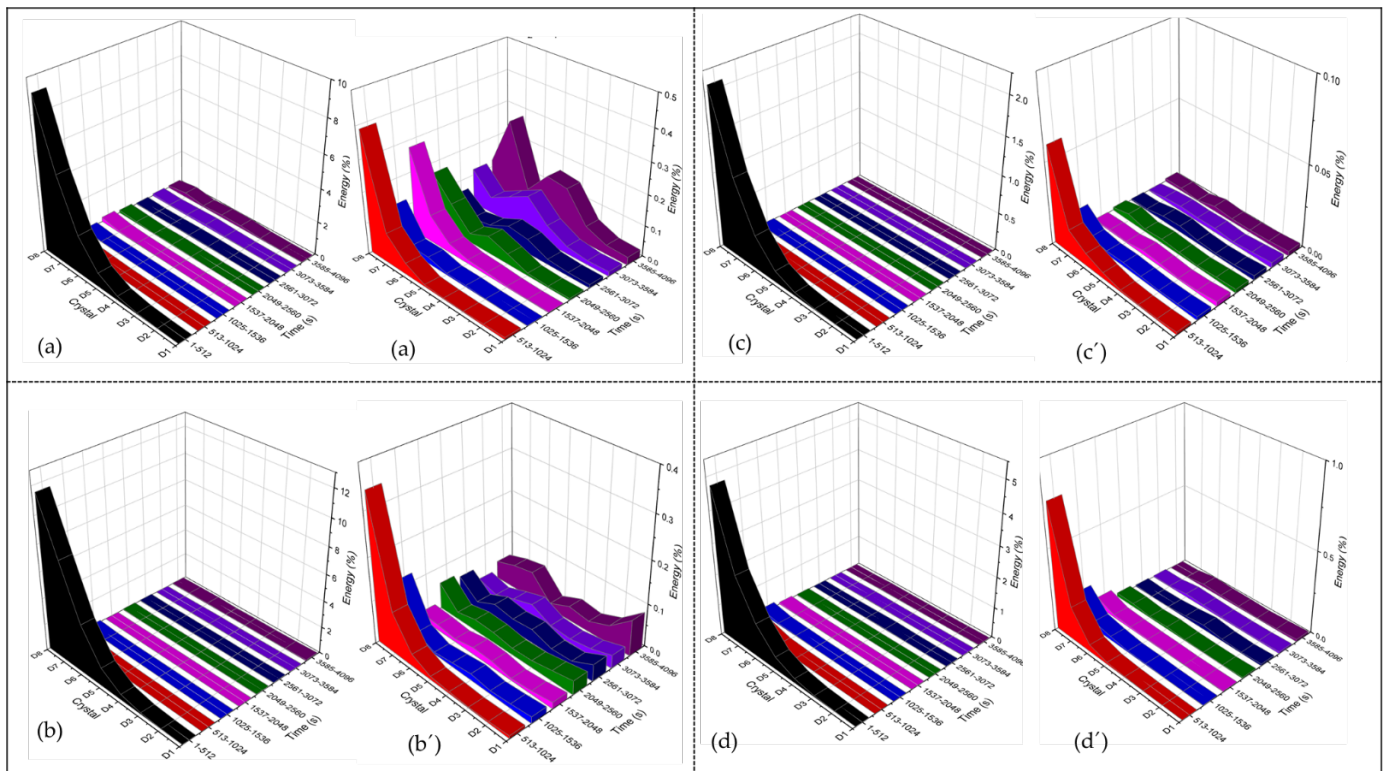
Figure 11 presents the wavelets analysis for the anodized Ti-6Al-2Sn-4Zr-2Mo. In Figure 11a,b and d, the energy distribution is in the middle crystal, so the current is not distributed uniformly; this may be due to the difference in porosity in anodizing. Only the sample anodized in  $H_3PO_4$  and exposed to NaCl presented high energy in the first time-lapse, and, after that, the energy decreased to a passivate system. This behavior is related to pore diameter, where  $Cl^-$  can penetrate.



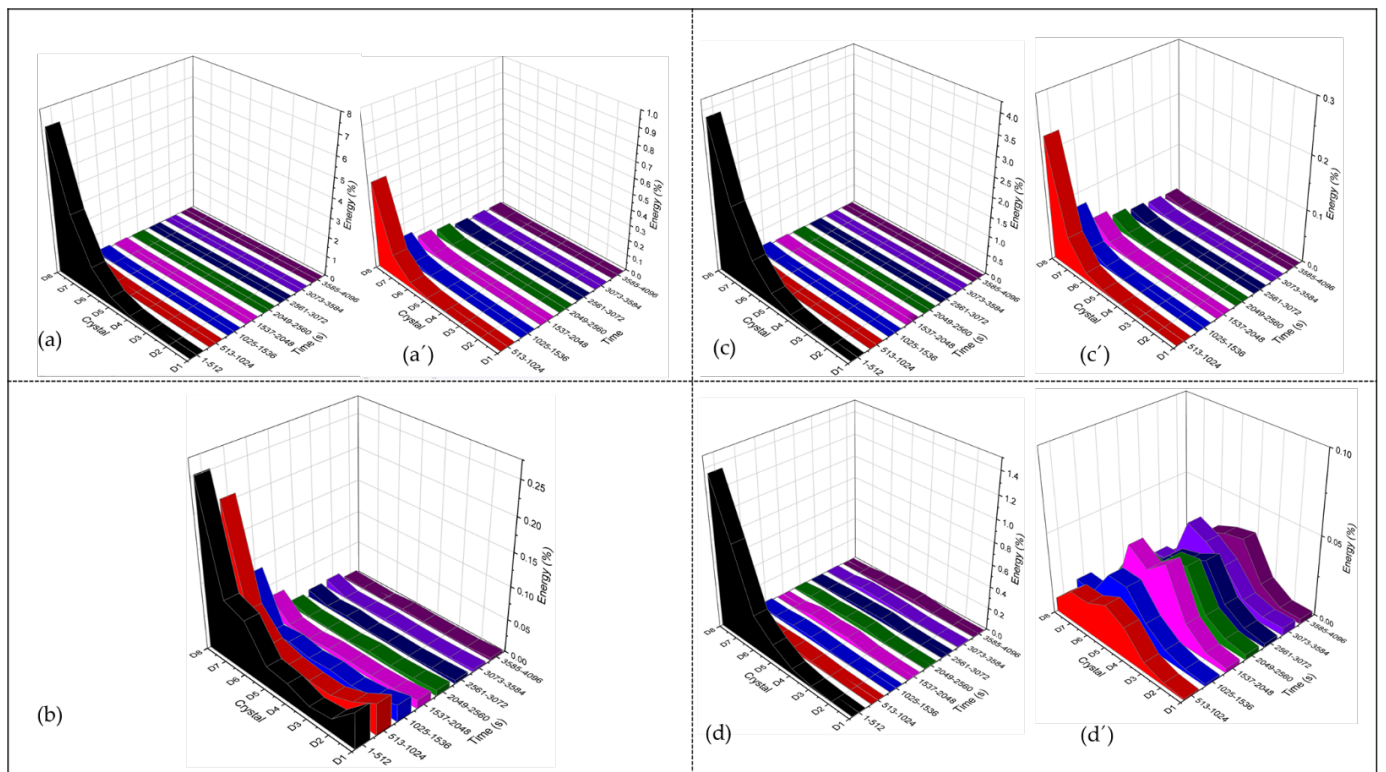
**Figure 11.** Wavelets analysis for Ti-6Al-2Sn-4Zr-2Mo anodized immersed in 3.5% wt. NaCl and  $H_2SO_4$  solutions. (a,c)  $H_2SO_4$  bath and (b,d)  $H_3PO_4$  bath.

Figure 12 shows the behavior of anodized Ti-6Al-4V by wavelets analysis. Figure 12a–d in the time-lapse of 1–512 and 513 to 1024 s presents a higher energy accumulation in the middle and last crystals; this behavior is related to non-homogenous porosity (middle crystals) and diffusion of the process. In the windowing of 12 (a'), the behavior is ad hoc for diffusion. In the time-lapse of 3585–4096 s (purple), energy accumulates in the middle crystal, and the corrosion process predominates localization due to the dissolution of specific zones in anodization. In Figure 12b'–d', energy is accumulated equitably, which occurs in a passive system.

Figure 13 shows the wavelets analysis for anodized Ti Beta-C. In the first time-lapses (black and blue graphics), Figure 13a–d presents the higher accumulation in crystals D7 and D8; this behavior is related to a uniform distribution and similar sizes of the pores. After making a windowing, Figure 10a' show low energy distribution on all crystal, related to a passive system in that media. Only Figure 10d' shows energy accumulation in the middle crystals; this behavior is related to the non-uniform dissolution of material by  $OH^-$ , which is due to the probable formation of different types of oxides in the surface layer. Hence, oxides of different elements degrade first and provoke the localization process.



**Figure 12.** Wavelets analysis for Ti-6Al-4V anodized immersed in 3.5% wt. NaCl and H<sub>2</sub>SO<sub>4</sub> solution. (a,c) H<sub>2</sub>SO<sub>4</sub> bath (b,d) H<sub>3</sub>PO<sub>4</sub> bath and (a'–d') windowing of wavelets analysis.



**Figure 13.** Wavelets analysis for Ti Beta-C anodized immersed in 3.5% wt. NaCl and H<sub>2</sub>SO<sub>4</sub> solutions. (a,c) H<sub>2</sub>SO<sub>4</sub> bath (b,d) H<sub>3</sub>PO<sub>4</sub> bath and (a',c',d') windowing of wavelets analysis.

#### 4. Discussion

Alloying elements play an essential role in the corrosion resistance of titanium alloys, and the porosity in these alloys tends to compromise the mechanical strength. The SEM microstructures of titanium alloys in the initial condition all show porosity; this causes a decrease in the mechanical properties since the pores can be stress concentrators and generate cracks [8,36,67]. Porosity makes the material susceptible to localized corrosion, although it can also re-passivate [37,67]. The samples in this research have porosity, leading to a lower corrosion potential value. The smaller pores help prevent diffusion of electrolytes and then lower the oxygen content, which is essential for the stability and conservation of the oxide layer on titanium [68].

This work is part of a project that has given results of alloys without coatings [36,52]. When alloys without anodizing were analyzed with PPC, the  $E_{\text{corr}}$  values reported were more negative, with an average difference of 0.200 V.  $I_{\text{corr}}$  values for alloys in non-anodized condition had values of  $\times 10^{-6}$  A/cm<sup>2</sup>. When anodized,  $i_{\text{corr}}$  values vary from  $\times 10^{-7}$  to  $\times 10^{-9}$  A/cm<sup>2</sup>. Additionally, PSD  $\Psi^0$  values are higher for metals without anodizing, while in anodizing conditions values change from a range of  $-138/-122$  dBi (A<sup>2</sup>·Hz<sup>-1</sup>)<sup>1/2</sup> to  $-131/-180$  dBi (A<sup>2</sup>·Hz<sup>-1</sup>)<sup>1/2</sup>. These results indicate an improvement in the behavior of the anodized samples, reducing the corrosion kinetics.

The electrochemical behavior of the anodized samples analyzed with CCP showed the absence of a positive hysteresis loop, which implies that localized corrosion does not occur but could indicate an active surface and general corrosion. A positive hysteresis is related to pitting and crevice corrosion.

The absorption of Cl<sup>-</sup> will depend on the surface charge [69–73]. If the charge is positive, it is easier for Cl<sup>-</sup> diffusion or an adsorption process to occur. Anodized Ti-6Al-4V and Ti Beta-C samples presented a long duration process in wavelet analysis because the charge (and  $E_{\text{corr}}$ ) have positive values (see Table 2). The diffusion process is helped by porosity. Since anodized Ti-6Al-4V and Ti Beta-C samples showed smaller porosity diameter than other samples, a capillary phenomenon helps Cl<sup>-</sup> diffusion.

It is important to consider that Cl<sup>-</sup> acts as an interstitial element, so if the anodizing pores are small, the Cl<sup>-</sup> will have problems penetrating the surface [74,75]. The presence of Cl<sup>-</sup> induces localized corrosion, with ions migrating across the passive film. When oxychloride accumulates at the interface metal-layer, the passive layer will break down and generate a pitting [76–82]. In this research, the anodized layer did not break; nevertheless, under electrolyte exposure (NaCl solution), the mechanism occurs in the anodized and oxide layer interface.

Song et al. [83] reported the effects of spark anodizing treatment on Ti alloys exposed to saline solution. Titanium with vanadium as an alloying element showed less corrosion resistance due to the dissolution of a vanadium oxide layer. This case is reflected in Ti-6Al-4V and Ti Beta-C anodized in H<sub>2</sub>SO<sub>4</sub> solution, even in CPP and EN (wavelets). In CPP, the passivation breakdown potential is lower than the other anodized samples. In wavelets, the energy accumulation in middle crystals is related to a localized process (breakdown of vanadium oxide layer).

On the other hand, ions such as H<sup>+</sup>, OH<sup>-</sup>, or SO<sub>4</sub> are smaller and can generate passive layers or cathodic reactions. For this reason, when samples are exposed to 3.5% wt. H<sub>2</sub>SO<sub>4</sub> they show high activity in the middle crystals because the cathodic reaction has been measured. However, H<sub>2</sub>SO<sub>4</sub> can create instability in the development of porosity [84,85]. Generating a good passivation is necessary to take care of the material surface. If porosity increases, the anodization could be poorer [86]. The effect of the OH<sup>-</sup> ion is present in Ti Beta-C anodized in sulfuric acid and immersed in 3.5% wt. H<sub>2</sub>SO<sub>4</sub> solution (Figure 6a): the anodized passive layer formed is broken, and presents instability on the surface due to OH<sup>-</sup> evolution. Figure 14 shows a diagram with the corrosion mechanism of titanium and its anodized alloys in acid baths.

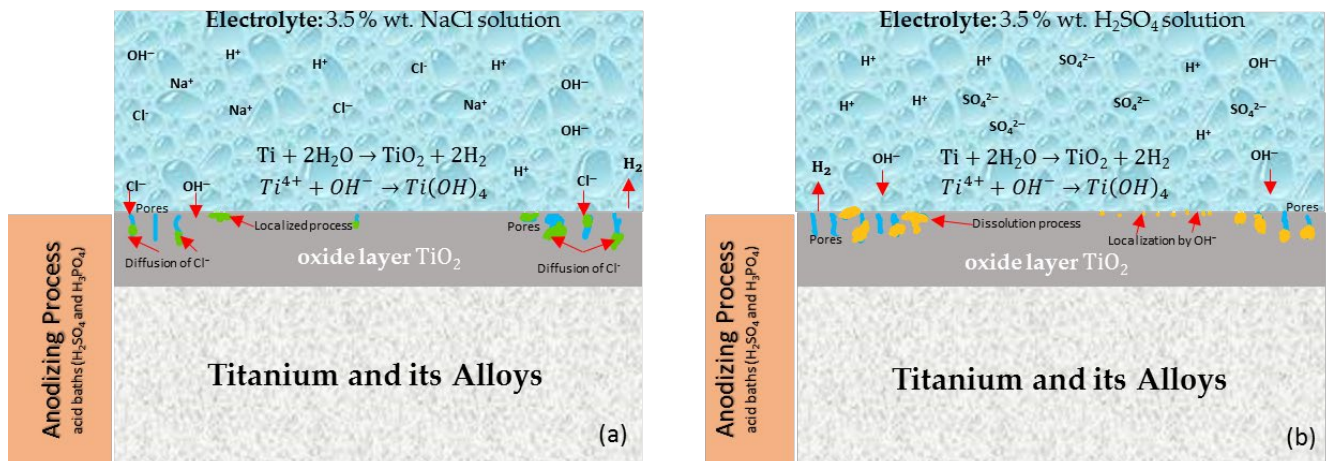
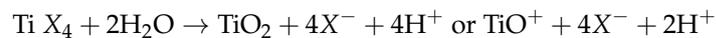


**Figure 14.** Schematic diagram of anodizing process for titanium and its alloys exposed to 3.5% wt. NaCl and H<sub>2</sub>SO<sub>4</sub> solutions: (a) H<sub>2</sub>SO<sub>4</sub> bath; (b) H<sub>3</sub>PO<sub>4</sub> bath.

Nevertheless, the alloys did not show high porosity. Current and pH affect the porosity level; as the current increases, the porosity was more significant [82]. A high porosity level is associated with high current and voltage values [85–87], so high current density is related to high porosity. However, a high current allows a rapid formation of the oxide layer. The anodizing time will be reduced in future research to reduce the porosity level.

Prando et al. [88] investigated the behavior of titanium anodized in halides (Cl<sup>−</sup>, Br<sup>−</sup>, F<sup>−</sup>, etc.) and proposed the reaction



where  $X$  is a halide. When the solution is in steady-state, water is the only species transported into the pit, and TiO<sub>2</sub> and H<sup>+</sup> are transported out. The reaction generated in the titanium oxide layer permeates the surface and breaks the oxide layer's dielectric resistance.

Additionally, Prando et al. [89,90] reported that a high current reduces the anodizing time, irrespective of the pH solution. Moreover, these authors conclude that alloying with Nb, Pd, or elements of the Cr group increase the corrosion resistance, as is the case of Ti Beta-C. Adding a beta stabilizer can help reduce the percentage of porosity in the anodized samples of Ti-6Al-4V. In fact, in the present work, Ti Beta-C presented a lower percentage of porosity.

Chien et al. [91] reported micropores in the Ti-anodized surface, and they attributed this to the multiple micro-arc discharges that occur in the anodization. Chamanzadeh et al. [92] obtained porous surfaces, but they concluded that an aggressive reaction of oxygen may have burned off the anodizing. In addition, with regards to the change related to the amount of energy to do the anodizing with a distance between pores, if the energy required is high, then the distance between pores will be greater. It is notable in images 2 and 3 that the distance between pores is greater when anodized in H<sub>3</sub>PO<sub>4</sub> due to the oxygen reaction.

Mizukoshi and Masahashi [93] related porosity and distribution to acid concentration; the porosity diameter increases with increasing acid concentration. Our anodized sulfuric acid has a higher pH, so the presence of pores increases (in images 2 and 3 it is interesting to see that there are more pores with the anodizing in H<sub>2</sub>SO<sub>4</sub>). However, the pore diameter for samples anodized in H<sub>3</sub>PO<sub>4</sub> is greater due to oxygen reactions. The acid media accelerate the process of pore generation. Thus, the number of pores is likely to decrease if the anodizing time decreases.

Laurindo et al. [94] found that porosity and pore size increase with current density and thickness when a high current is applied. Moreover, cracks can be generated, as in Ti Beta-C in both anodizing systems. In this research, cracks are probably only on the

anodizing surface due to the electrochemical behavior shown. However, if the anodizing time increases, the cracks may propagate into the substrate, thus decreasing the anodizing properties. Additionally, Zhang et al. [95] found that the sizes of pores or tubes is directly dependent on ionic current.

Research by Mazzarolo et al. [96] concluded that an amorphous layer is created. When the electrolyte penetrates the cavities, the localization process occurs, and the passive layer growth will occur in preference zones (see Figure 14).

Authors such as Thompson et al. and Diamanti et al. [97,98] related the electrolyte with the type of oxide generated. They associated being anodized in  $H_2SO_4$  with anatase; this is an important field of research for future works to relate the electrochemical behavior with the type of passive layer and crystal structure.

## 5. Conclusions

- The results indicated that the titanium alloys anodized in  $H_2SO_4$  showed a homogeneous surface morphology with fine pores. However, samples anodized in  $H_3PO_4$  showed a heterogeneous distribution with larger pore sizes but with fewer pores. This behavior is related to the reaction of oxygen in the  $H_3PO_4$  bath. Additionally, pore nucleation is associated with a higher pH value in the  $H_2SO_4$  bath.
- The percentage of porosity decreased in alloys with a higher amount of beta stabilizers.
- CPP results revealed that the Ti Beta-C alloy had a higher corrosion resistance but a lower passivity range than the other anodized alloys; this behavior may be related to the formation of cracks in the anodized surface. Although the EN technique shows a stable behavior in wavelets analysis, and since this is a non-perturbative technique, the energy necessary to start the anodizing dissolution was not enough. However, the anodizing in  $H_3PO_4$  showed higher activity in the middle crystal than in the  $H_2SO_4$  bath because pores are larger, generating diverse reactions more easily.
- The CPP technique indicated that for anodized titanium and anodized titanium alloys, lower corrosion current densities ( $i_{corr}$ ), and negative hysteresis was observed for all samples. Thus, the process provides excellent corrosion resistance.
- Increasing porosity in titanium alloys increases the corrosion kinetics, particularly if pores are tiny. This behavior is observed in a more significant way for the anodized Ti-6Al-2Sn-4Zr-2Mo alloy in  $H_2SO_4$ , which presented higher porosity, fine pores, and an increase in the corrosion kinetics.
- Results show that the roughness of the anodize increase with the presence of beta-phase forming alloying elements in titanium.
- Electrochemical noise is a suitable technique to characterize the corrosion behavior, as well as the uniformity of the anodizing surface. The technique can also determine how homogenous the anodized layer is in the first seconds of the process. The wavelet method (in the time-frequency domain) allows us to determine that the energy accumulated in the middle crystal may be related to a heterogeneous pore distribution.
- Noise impedance ( $Z_n$ ) shows similar behavior for Ti-6Al-2Sn-4Zr-2Mo (anodized on  $H_3PO_4$ ) and Ti Beta-C (anodized in both media) in relation to corrosion resistance as determined by the CPP technique. Therefore, the application of both methods is suitable to determine the corrosion kinetics of passive systems.
- The results by PSD in current for the anodized Ti CP2 and Ti-6Al-4V alloys showed the higher dissolution. These results correlate well with those obtained with the CPP technique.
- Anodization of Ti CP2 and Ti-6Al-4V alloys exposed in both media ( $NaCl$  and  $H_2SO_4$ ) showed homogenous porosity and the largest pore size. This characteristic may be associated with the high dissolution of the anodizing shown by the PSD in current and CPP methods.

**Author Contributions:** Conceptualization, F.A.-C., J.M.J.-M. and C.G.-T.; methodology, J.M.J.-M., A.D.D., J.P.F.-D.I.R. and J.C.-M., data curation, F.A.-C., J.M.J.-M., J.C.-N., E.M.-B. and D.N.-M. formal analysis, J.C.-M., F.A.-C., P.B. and C.G.-T. writing—review and editing, F.A.-C., J.M.J.-M., J.C.-N. and C.G.-T. All authors have read and agreed to the published version of the manuscript.

**Funding:** This research was funded by the Mexican National Council for Science and Technology (CONACYT) through projects A1-S-8882 and Universidad Autónoma de Nuevo León (UANL).

**Institutional Review Board Statement:** Not applicable.

**Informed Consent Statement:** Not applicable.

**Data Availability Statement:** Not applicable.

**Acknowledgments:** The authors wish to thank The Academic Body UANL—CA-316 “Deterioration and integrity of composite materials”, and thank Maria Lara for her support in the SEM analysis.

**Conflicts of Interest:** The authors declare no conflict of interest.

## References

1. Izmir, M.; Ercan, B. Anodization of titanium alloys for orthopedic applications. *Front. Chem. Sci. Eng.* **2019**, *13*, 28. [[CrossRef](#)]
2. Gloria, A.; Montanari, R.; Richetta, M.; Varone, A. Alloys for aeronautic applications: State of the art and perspectives. *Metals* **2019**, *9*, 662. [[CrossRef](#)]
3. Peters, M.; Kumpfert, J.; Ward, C.H.; Lleyends, C. Titanium alloys for aerospace applications. *Adv. Eng. Mater.* **2003**, *5*, 419. [[CrossRef](#)]
4. Veiga, C.; Davim, J.P.; Loureiro, A.J.R. Properties and applications of titanium alloys: A brief review. *Rev. Adv. Mater. Sci.* **2012**, *32*, 133.
5. Apaza-Bedoya, K.; Tarce, M.; Benfatti, C.A.M.; Henriques, B.; Mathew, M.T.; Teughels, W.; Souza, J.C.M. Synergistic interactions between corrosion and wear at titanium-based dental implant connections: A scoping review. *J. Periodontal Res.* **2017**, *52*, 946–954. [[CrossRef](#)]
6. Cordeiro, J.M.; Barão, V.A.R. Is there scientific evidence favoring the substitution of commercially pure titanium with titanium alloys for the manufacture of dental implants? *Mater. Sci. Eng. C* **2017**, *71*, 1201–1215. [[CrossRef](#)]
7. Noronha Oliveira, M.; Schunemann, W.V.H.; Mathew, M.T.; Henriques, B.; Magini, R.S.; Teughels, W.; Souza, J.C.M. Can degradation products released from dental implants affect peri-implant tissues? *J. Periodontal Res.* **2017**, *6*, 1–11. [[CrossRef](#)] [[PubMed](#)]
8. Bocchetta, P.; Chen, L.-Y.; Tardelli, J.D.C.; Reis, A.C.D.; Almeraya-Calderón, F.; Leo, P. Passive layers and corrosion resistance of biomedical Ti-6Al-4V and  $\beta$ -Ti alloys. *Coatings* **2021**, *11*, 487. [[CrossRef](#)]
9. Alam, M.J.; Cameron, D.C. Preparation and characterization of TiO<sub>2</sub> thin films by sol-gel method. *J. Sol-Gel Sci. Technol.* **2002**, *25*, 137–145. [[CrossRef](#)]
10. Diamanti, M.V.; Codeluppi, S.; Cordioli, A.; Pedefferri, M.P. Effect of thermal oxidation on titanium oxides characteristics. *J. Exp. Nanosci.* **2009**, *4*, 365–372. [[CrossRef](#)]
11. Lobl, P.; Huppertz, M.; Mergel, D. Nucleation and growth in TiO<sub>2</sub> films prepared by sputtering and evaporation. *Thin Solid Film* **1994**, *251*, 72–79. [[CrossRef](#)]
12. Dziejowski, P.M.; Grzeszczuk, M. Deposition of thin TiO<sub>2</sub> layers on platinum by means of cyclic voltammetry of selected complex Ti (IV) media leading to anatase. *Electrochim. Acta* **2009**, *54*, 4045–4055. [[CrossRef](#)]
13. Ma, K.; Zhang, R.; Sun, J.; Liu, S. Oxidation mechanism of biomedical titanium alloy surface and experiment. *Int. J. Corros.* **2020**, *2020*, 1678615. [[CrossRef](#)]
14. Benea, L.; Celis, J.P. Reactivity of porous titanium oxidefilm and chitosan layer electrochemically formed on Ti-6Al-4V alloy in biological solution. *Surf. Coat. Technol.* **2018**, *354*, 145–152. [[CrossRef](#)]
15. Zhang, L.-C.; Chen, L.-Y.; Wang, L. Surface modification of titanium and titanium alloys: Technologies, developments, and future interests. *Adv. Eng. Mater.* **2020**, *22*, 1901258. [[CrossRef](#)]
16. Dias Corpa Tardelli, J.; Lima da Costa Valente, M.; Theodoro de Oliveira, T.; Cândido dos Reis, A. Influence of chemical composition on cell viability on titanium surfaces: A systematic review. *J. Prosthet. Dent.* **2021**, *125*, 421–425. [[CrossRef](#)]
17. Peñarrieta-Juanito, G.; Sordi, M.B.; Henriques, B.; Dotto, M.E.R.; Teughels, W.; Silva, F.S.; Magini, R.S.; Souza, J.C.M. Surface damage of dental implant systems and ions release after exposure to fluoride and hydrogen peroxide. *J. Periodontal Res.* **2018**, *54*, 46–52. [[CrossRef](#)]
18. Michalska-Domanska, M.; Łazinska, M.; Łukasiewicz, J.; Mol, J.M.C.; Durejko, T. Self-organized anodic oxides on titanium alloys prepared from glycol- and glycerol-based electrolytes. *Materials* **2020**, *13*, 4743. [[CrossRef](#)]
19. Gulati, K.; Sinn Aw, M.; Findlay, D.; Losic, D. Local drug delivery to the bone by drug-releasing implants: Perspectives of nano-engineered titania nanotube arrays. *Ther. Deliv.* **2012**, *3*, 857–873. [[CrossRef](#)]

20. Luz, A.R.; Santos, L.S.; Lepienski, C.M.; Kuroda, P.B.; Kuromoto, N.K. Characterization of the morphology, structure and wettability of phase dependent lamellar and nanotube oxides on anodized Ti-10Nb alloy. *Appl. Surf. Sci.* **2018**, *448*, 30–40. [[CrossRef](#)]
21. Dikicia, T.; Erola, M.; Toparlia, M.; Celika, E. Characterization and photocatalytic properties of nanoporous titanium dioxide layer fabricated on pure titanium substrates by the anodic oxidation process. *Ceram. Int.* **2014**, *40*, 1587–1591. [[CrossRef](#)]
22. Cabral-Miramontes, J.A.; Barceinas-Sánchez, J.D.O.; Poblano-Salas, C.A.; Pedraza-Basulto, G.K.; Nieves-Mendoza, D.; Zambrano-Robledo, P.C.; Almeraya-Calderón, F.; Chacón-Nava, J.G. Corrosion behavior of AISI 409Nb stainless steel manufactured by powder metallurgy exposed in H<sub>2</sub>SO<sub>4</sub> and NaCl solutions. *Int. J. Electrochem. Sci.* **2013**, *8*, 564–577.
23. Hai, L.; Gou-qiang, X.; Pan, Z.; Hua-sen, Z.; Kan, M.Y. The Hilbert–Huang transform-based denoising method for the TEM response of a PRBS source signal. *Pure Appl. Geophys.* **2016**, *173*, 2777–2789. [[CrossRef](#)]
24. Blasco-Tamarit, E.; Igual-Muñoz, A.; García Antón, J.; García-García, D. Galvanic corrosion of titanium coupled to welded titanium in LiBr solutions at different temperatures. *Corros. Sci.* **2009**, *51*, 1095–1102. [[CrossRef](#)]
25. Wang, Z.B.; Hu, H.X.; Zheng, Y.G. Synergistic effects of fluoride and chloride on general corrosion behavior of AISI 316 stainless steel and pure titanium in H<sub>2</sub>SO<sub>4</sub> solutions. *Corros. Sci.* **2018**, *130*, 203–217. [[CrossRef](#)]
26. Rao, B.M.; Torabi, A.; Varghese, O.K. Anodically grown functional oxide nanotubes and applications. *MRS Commun.* **2016**, *6*, 375–396. [[CrossRef](#)]
27. Sul, Y.-T.; Johansson, C.B.; Petronis, S.; Krozer, A.; Jeong, Y.; Wennerberg, A.; Albrektsson, T. Characteristics of the surface oxides on turned and electrochemically oxidized pure titanium implants up to dielectric breakdown. *Biomaterials* **2002**, *23*, 491–501. [[CrossRef](#)]
28. Takemoto, S.; Hattori, M.; Yoshinari, M.; Kawada, E.; Oda, Y. Corrosion behavior and surface characterization of titanium in solution containing fluoride and albumin. *Biomaterials* **2005**, *26*, 829–837. [[CrossRef](#)]
29. Regonini, D.; Bowen, C.R.; Jaroenworuluck, A.; Stevens, R. A review of growth mechanism, structure and crystallinity of anodized TiO<sub>2</sub> nanotubes. *Mater. Sci. Eng. R Rep.* **2013**, *74*, 377–406. [[CrossRef](#)]
30. Jaroenworuluck, A.; Regonini, D.; Bowen, C.; Stevens, R.; Allsopp, D. Macro, micro and nanostructure of TiO<sub>2</sub> anodised films prepared in a fluorine-containing electrolyte. *J. Mater. Sci.* **2007**, *42*, 6729–6734. [[CrossRef](#)]
31. Jelliti, S.; Richard, C.; Retraint, D.; Roland, T.; Chemkhi, M.; Demangel, C. Effect of surface nanocrystallization on the corrosion behavior of Ti-6Al-4V titanium alloy. *Surf. Coat. Technol.* **2013**, *224*, 82–87. [[CrossRef](#)]
32. Ji, R.; Wang, B.; Jin, H.; Liu, Y.; Cheng, W.; Cai, B.; Li, X. Removing loose oxide layer and producing dense  $\alpha$ -phase layer simultaneously to improve corrosion resistance of Ti-6Al-4V titanium alloy by coupling electrical pulse and ultrasonic treatment. *Surf. Coat. Technol.* **2020**, *384*, 125329. [[CrossRef](#)]
33. Risking, J.; Khentov, A. *Electrocorrosion and Protection of Metals*, 2nd ed.; Risking, J., Ed.; Elsevier: Amsterdam, The Netherlands, 2019; pp. 225–248.
34. Kuphasuk, C.; Oshida, Y.; Andres, C.J.; Hovijitra, S.T.; Barco, M.T.; Brown, D.T. Electrochemical corrosion of titanium and titanium-based alloys. *J. Prothet. Dent.* **2001**, *85*, 195–202. [[CrossRef](#)]
35. Pink, H.; Rui, S.; Kuaishe, W.; Fan, Y.; Boliang, H.; Zhen-Lu, C.; Qinwe, L.; Weicheng, C.; Dongxin, L.; Lei, G.; et al. Electrochemical corrosion behavior of titanium-zirconium-molybdenum alloy. *Rare Met. Mater. Eng.* **2017**, *46*, 1225–1230. [[CrossRef](#)]
36. Jaquez-Muñoz, J.; Gaona-Tiburcio, C.; Lira-Martinez, A.; Zambrano-Robledo, P.; Maldonado-Bandala, E.; Samaniego-Gamez, O.; Nieves-Mendoza, D.; Olguin-Coca, J.; Estupiñan-Lopez, F.; Almeraya-Calderon, F. Susceptibility to pitting corrosion of Ti-CP2, Ti-6Al-2Sn-4Zr-2Mo, and Ti-6Al-4V alloys for aeronautical applications. *Metals* **2021**, *11*, 1002. [[CrossRef](#)]
37. Jáquez-Muñoz, J.M.; Gaona-Tiburcio, C.; Cabral-Miramontes, J.; Nieves-Mendoza, D.; Maldonado-Bandala, E.; Olguin-Coca, J.; López-Léon, L.D.; Flores-De los Rios, J.P.; Almeraya-Calderón, F. Electrochemical noise analysis of the corrosion of titanium alloys in NaCl and H<sub>2</sub>SO<sub>4</sub> solutions. *Metals* **2021**, *11*, 105. [[CrossRef](#)]
38. Galván-Martínez, R.; Cabrera-de la Cruz, D.; Contreras, A.; Orozco-Cruz, R. A novel experimental arrangement for corrosion study of X60 pipeline steel weldments at turbulent flow conditions. *Corros. Eng. Sci. Technol.* **2016**, *51*, 400–407. [[CrossRef](#)]
39. Galván-Martínez, R.; Orozco-Cruz, R.; Torres-Sanchez, R.; Martínez, E.A. Corrosion study of the X52 steel immersed in seawater with a corrosion inhibitor using a rotating cylinder electrode. *Mater. Corros.* **2010**, *61*, 872–876. [[CrossRef](#)]
40. Soltis, J. Passivity breakdown, pit initiation and propagation of pits in metallic materials—Review. *Corros. Sci.* **2015**, *90*, 5–22. [[CrossRef](#)]
41. Noel, J.J.; Shoesmith, D.W.; Ebrahimi, N. *Corrosion of Titanium, and Its Alloys*, 1st ed.; Wandelt, K., Ed.; Elsevier: Amsterdam, The Netherlands, 2016; pp. 193–199.
42. Seo, D.; Lee, J.B. Effects of competitive anion adsorption (Br<sup>−</sup> or Cl<sup>−</sup>) and semiconducting properties of the passive films on the corrosion behavior of the additively manufactured Ti-6Al-4V alloys. *Corros. Sci.* **2020**, *173*, 108789. [[CrossRef](#)]
43. Tafel, J. Über die polarization bei kathodischer wasserstoffentwicklung. *Z. Phys. Chem.* **1905**, *50*, 641–712. [[CrossRef](#)]
44. Attabi, S.; Mokhtari, M.; Taibi, Y.; Abdel-Rahman, I.; Hafez, B.; Elmsellem, H. Electrochemical and tribological behavior of surface-treated titanium alloy Ti-6Al-4V. *J. Bio-Tribo-Corros.* **2019**, *5*, 2. [[CrossRef](#)]
45. Orazem, E.N.; Tribollet, B. *Electrochemical Impedance Spectroscopy*; John Wiley & Sons, Inc.: Hoboken, NJ, USA, 2017.
46. Wagner, C.; Traud, W. *Über die Deutung von Korrosionsvorgängen durch Überlagerung von Elektrochemischen Teilvorgängen und über die Potentialbildung an Mischelektroden*, *Z. Elektrochem*; Springer: Berlin/Heidelberg, Germany, 1951; pp. 391–454.

47. Butler, J.A.V. Studies in heterogeneous equilibria. Part II—The kinetic interpretation on the Nernst theory of electromotive force. *Trans. Faraday Soc.* **1924**, *19*, 729–733. [[CrossRef](#)]
48. Monticelli, C. Evaluation of corrosion inhibitors by electrochemical noise analysis. *J. Electrochem. Soc.* **1992**, *139*, 706. [[CrossRef](#)]
49. Park, C.J.; Kwon, H.S. Electrochemical noise analysis of localized corrosion of duplex stainless steel aged at 475 °C. *Mater. Chem. Phys.* **2005**, *91*, 355–360. [[CrossRef](#)]
50. Suresh, G.U.; Kamachi, M.S. Electrochemical noise analysis of pitting corrosion of type 304L stainless steel. *Corrosion* **2014**, *70*, 283–293. [[CrossRef](#)]
51. Cottis, R.; Turgoose, S.; Mendoza-Flores, J. The effects of solution resistance on electrochemical noise resistance measurements: A theoretical analysis. In *Electrochemical Noise Measurement for Corrosion Applications STP 1277*; Kearns, J.R., Scully, J.R., Roberge, P.R., Reirchert, D.L., Dawson, L., Eds.; ASTM International, Materials Park: West Conshohocken, PA, USA, 1996; pp. 93–100.
52. Eden, D.A. Electrochemical noise—The first two octaves. In *Corrosion/98*; NACE: San Diego, CA, USA, 1998; pp. 1–31.
53. Coakley, J.; Vorontsov, V.A.; Littlell, K.C.; Heenan, R.K.; Ohnuma, G.; Jones, N.G.; Dye, D. Nanoprecipitation in a beta-titanium alloy. *J. Alloys Compd.* **2015**, *623*, 146. [[CrossRef](#)]
54. ASTM E3-95. *Standard Practice for Preparation of Metallographic Specimens*; ASTM International: West Conshohocken, PA, USA, 1995.
55. ASTM E407-07. *Standard Practice for Microetching Metals and Alloys*; ASTM International: West Conshohocken, PA, USA, 2011.
56. AMS2487. *Anodic Treatment of Titanium and Titanium Alloys Solution pH 12.4 Maximum*; SAE International: Warrendale, PA, USA, 2018.
57. Cabral-Miramontes, J.; Gaona-Tiburcio, C.; Estupiñán-López, F.; Lara-Banda, M.; Zambrano-Robledo, P.; Nieves-Mendoza, D.; Maldonado-Bandala, E.; Chacón-Nava, J.; Almeraya-Calderón, F. Corrosion resistance of hard coat anodized AA 6061 in citric-sulfuric solutions. *Coatings* **2020**, *10*, 601. [[CrossRef](#)]
58. Cabral-Miramontes, J.A.; Gaona-Tiburcio, C.; Almeraya-Calderón, F.; Estupiñán-Lopez, H.F.; Pedraza-Basulto, G.; Poblano-Salas, C. Parameter studies on high-velocity oxy-fuel spraying of CoNiCrAlY coatings used in the aeronautical industry. *Int. J. Corros.* **2014**, *2014*, 703806. [[CrossRef](#)]
59. ASTM G5-11. *Standard Reference Test Method for Making Potentiostatic and Potentiodynamic Anodic Polarization Measurements*; ASTM International: West Conshohocken, PA, USA, 2011.
60. ASTM G61-86 (2018). *Standard Test Method for Conducting Cyclic Potentiodynamic Polarization Measurements for Localized Corrosion Susceptibility of Iron-, Nickel-, or Cobalt-Based Alloys*; ASTM International: West Conshohocken, PA, USA, 2018.
61. Lara-Banda, M.; Gaona-Tiburcio, C.; Zambrano-Robledo, P.; Delgado, E.M.; Cabral-Miramontes, J.A.; Nieves-Mendoza, D.; Maldonado-Bandala, E.; Estupiñán-López, F.; Chacón-Nava, J.G.; Almeraya-Calderón, F. Alternative to nitric acid passivation of 15-5 and 17-4PH stainless steel using electrochemical techniques. *Materials* **2020**, *13*, 2836. [[CrossRef](#)] [[PubMed](#)]
62. Homborg, A.M.; Cottis, R.A.; Mol, J.M.C. An integrated approach in the time, frequency and time-frequency domain for the identification of corrosion using electrochemical noise. *Electrochim. Acta* **2016**, *222*, 627–640. [[CrossRef](#)]
63. Gaona-Tiburcio, C.; Aguilar, L.M.R.; Zambrano-Robledo, P.; Estupiñán-López, F.; Cabral-Miramontes, J.A.; Nieves-Mendoza, D.; Castillo-González, E.; Almeraya-Calderón, F. Electrochemical noise analysis of nickel based superalloys in acid solutions. *Int. J. Electrochem. Sci.* **2014**, *9*, 523–533.
64. Montoya-Rangel, M.; de Garza-Montes, O.N.; Gaona-Tiburcio, C.; Colás, R.; Cabral-Miramontes, J.; Nieves-Mendoza, D.; Maldonado-Bandala, E.; Chacón-Nava, J.; Almeraya-Calderón, F. Electrochemical noise measurements of advanced high-strength steels in different solutions. *Metals* **2020**, *10*, 1232. [[CrossRef](#)]
65. Dawson, D.L. Electrochemical noise measurement: The definitive in-situ technique for corrosion applications? In *Electrochemical Noise Measurement for Corrosion Applications STP 1277*; Kearns, J.R., Scully, J.R., Roberge, P.R., Reirchert, D.L., Dawson, L., Eds.; ASTM International, Materials Park: West Conshohocken, PA, USA, 1996; pp. 3–39.
66. ASTM G199-09. *Standard Guide for Electrochemical Noise Measurement*; ASTM International: West Conshohocken, PA, USA, 2009.
67. Froes, F.; Quian, M. *Titanium for Consumer Applications. Real World Use of Titanium*; Elsevier Inc.: Amsterdam, The Netherlands, 2019; pp. 27–65. [[CrossRef](#)]
68. Seah, K.H.W.; Thampuran, R.; Teoh, S.H. The influence of pore morphology on corrosion. *Corros. Sci.* **1998**, *40*, 547–556. [[CrossRef](#)]
69. Mehdi-pour, M.; Naderi, R.; Markhali, B.P. Electrochemical study of effect of the concentration ofazole derivatives on corrosion behavior of stainless steel in H<sub>2</sub>SO<sub>4</sub>. *Prog. Org. Coat.* **2014**, *77*, 1761–1767. [[CrossRef](#)]
70. Bertocci, U.; Huet, F. Noise analysis applied to electrochemical systems. *Corrosion* **1995**, *51*, 131–144. [[CrossRef](#)]
71. Bertucci, U.; Gabrielli, C.; Huet, F.; Keddam, M.; Rousseau, P. Noise resistance applied to corrosion measurements: II. *Experimental tests. J. Electrochem. Soc.* **1997**, *144*, 37. [[CrossRef](#)]
72. Xia, D.-H.; Song, S.-Z.; Behnamian, Y. Detection of corrosion degradation using electrochemical noise (EN): Review of signal processing methods for identifying corrosion forms. *Corros. Eng. Sci. Technol.* **2016**, *51*, 527–544. [[CrossRef](#)]
73. Lee, C.C.; Mansfeld, F. Analysis of electrochemical noise data for a passive system in the frequency domain. *Corros. Sci.* **1998**, *40*, 959–962. [[CrossRef](#)]
74. Legat, A.; Dolecek, V. Corrosion monitoring system based on measurement and analysis of electrochemical noise. *Corrosion* **1995**, *51*, 295–300. [[CrossRef](#)]
75. Estupiñán-López, H.F.; Almeraya-Calderón, F.; Bautista Margulis, G.R.; Baltazar Zamora, M.A.; Martínez-Villafañe, A.; Uruchurtu, C.J.; Gaona-Tiburcio, C. Transient analysis of electrochemical noise for 316 and duplex 2205 stainless steels under pitting corrosion. *Int. J. Electrochem. Sci.* **2011**, *6*, 1785–1796.

76. Xia, D.; Qin, Z.; Song, Z.; Macdonald, D.; Luo, J. Combating marine corrosion on engineered oxide surface by repelling, blocking and capturing  $\text{Cl}^-$ : Mini review. *Corros. Commun.* **2021**, *2*, 1–7. [[CrossRef](#)]
77. Corral-Higuera, R.; Arredondo-Rea, P.; Neri-Flores, M.A.; Gómez-Soberón, J.M.; Almaral-Sánchez, J.L.; Castorena-González, J.C.; Almeraya-Calderón, F. Chloride ion penetrability and corrosion behavior of steel in concrete with sustainability characteristics. *Int. J. Electrochem. Sci.* **2011**, *6*, 958–970.
78. Martínez-Villafañe, A.; Chacon-Nava, J.G.; Gaona-Tiburcio, C.; Almeraya-Calderon, F.; Domínguez-Patiño, G.; Gonzalez-Rodríguez, G. Oxidation performance of a Fe–13Cr alloy with additions of rare earth elements. *Mater. Sci. Eng. A* **2003**, *363*, 15–19. [[CrossRef](#)]
79. Corral, H.R.; Arredondo, R.S.P.; Neri, F.M.; Gómez, S.J.M.; Almeraya, C.F.; Castorena, G.J.H.; Almaral, S.J. Sulfate attack and reinforcement corrosion in concrete with recycled concrete aggregates and supplementary cementing materials. *Int. J. Electrochem. Sci.* **2011**, *6*, 613–621.
80. Ramirez-Arteaga, A.M.; Gonzalez-Rodriguez, J.G.; Campillo, B.; Gaona-Tiburcio, C.; Dominguez-Patiño, G.; Leduc Lezama, L.; Chacon-Nava, J.G.; Neri-Flores, M.A.; Martinez-Villafañe, A. An electrochemical study of the corrosion behavior of a dual phase steel in 0.5M  $\text{H}_2\text{SO}_4$ . *Int. J. Electrochem. Sci.* **2010**, *5*, 1786–1798.
81. Pan, C.; Wang, X.; Behnamian, Y.; Wu, Z.; Qin, Z.; Xia, D.; Hu, W. Monododecyl phosphate film on LY12 aluminum alloy: pH-Controlled self-assembly and corrosion resistance. *J. Electrochem. Soc.* **2020**, *167*, 164510. [[CrossRef](#)]
82. Prando, D.; Branna, A.; Diamanti, M.V.; Beretta, S.; Bolzoni, F.; Ormellese, M.; Pedefferri, M. Corrosion of titanium: Part 1: Aggressive environments and man forms of degradation. *J. Appl. Biomater. Funct. Mater.* **2017**, *15*, e291–e302. [[CrossRef](#)] [[PubMed](#)]
83. Song, H.; Kim, M.; Jung, G.; Vang, M.; Park, Y. The effects of spark anodizing treatment of pure titanium metals and titanium alloys on corrosion characteristics. *Surf. Coat. Technol.* **2007**, *201*, 8738–8745. [[CrossRef](#)]
84. Homborg, A.M.; Tinga, T.; Zhang, X.; Van Westing, E.P.M.; Ferrari, G.M.; Wit, J.H.W.; Mol, J.M.W. A critical appraisal of the interpretation of electrochemical noise for corrosion studies. *Corrosion* **2017**, *70*, 971–987. [[CrossRef](#)]
85. Fattah-Alhosseini, A.; Attarzadeh, F.R.; Vakili-Azghandi, M. Effect of multi-pass friction stir processing on the electrochemical and corrosion behavior of pure titanium in strongly acidic solutions. *Metall. Mater. Trans. A* **2017**, *48*, 403–411. [[CrossRef](#)]
86. Martínez, C.; Guerra, C.; Silva, D.; Cubillos, M.; Briones, F.; Muñoz, L.; Páez, M.A.; Aguilar, C.; Sancy, M. Effect of porosity on mechanical and electrochemical properties of Ti-6Al-4V alloy. *Electrochim. Acta* **2020**, *338*, 135858. [[CrossRef](#)]
87. Karambakhsh, A.; Afshar, A.; Ghahramani, S.; Malekinejad, P. Pure commercial titanium color anodizing and corrosion resistance. *J. Mater. Eng. Perform.* **2011**, *20*, 1690–1696. [[CrossRef](#)]
88. Prando, D.; Nicolis, D.; Pedefferri, M.; Ormellese, M. Pitting corrosion on anodized titanium: Effect of halides. *Mater. Corros.* **2018**, *29*, 1441–1446. [[CrossRef](#)]
89. Prando, D.; Branna, A.; Diamanti, M.V.; Beretta, S.; Bolzoni, F.; Ormellese, M. Corrosion of titanium: Part 1: Effects of surface treatments. *J. Appl. Biomater. Funct. Mater.* **2018**, *16*, 3–13. [[CrossRef](#)]
90. Prando, D.; Branna, A.; Diamanti, M.V.; Beretta, S.; Bolzoni, F.; Ormellese, M. Electrochemical anodizing treatment to enhance localized corrosion resistance of pure titanium. *J. Appl. Biomater. Funct. Mater.* **2017**, *15*, e19–e24. [[CrossRef](#)] [[PubMed](#)]
91. Chien, C.; Hung, Y.; Hong, T.; Wu, C.; Kuo, T.; Lee, T.; Liao, T.; Lin, H.; Chuang, C. Preparation and characterization of porous bioceramic layers on pure titanium surface obtained by micro-arc oxidation process. *Appl. Phys. A* **2017**, *123*, 204. [[CrossRef](#)]
92. Chamanzadeh, Z.; Noormohammadi, M.; Zahedifar, M. Self-organized and uniform  $\text{TiO}_2$  nanotube arrays with optimized  $\text{NH}_4\text{F}$  concentration in electrolyte by high voltage electrochemical anodization. *Mater. Res. Express* **2018**, *5*, 55025. [[CrossRef](#)]
93. Mizukoshi, Y.; Masahashi, N. Fabrication of a  $\text{TiO}_2$  photocatalyst by anodic oxidation of Ti in an acetic acid electrolyte. *Surf. Coat. Technol.* **2014**, *240*, 226–232. [[CrossRef](#)]
94. Laurindo, C.A.H.; Torres, R.D.; Mali, S.A.; Gilbert, J.L.; Soares, P. Incorporation of Ca and P on anodized titanium surface: Effect of high current density. *Mater. Sci. Eng. C* **2014**, *37*, 223–231. [[CrossRef](#)]
95. Zhang, Y.; Fan, H.; Ding, X.; Yan, Q.; Wang, L.; Ma, W. Simulation of anodizing current-time curves and morphology evolution of  $\text{TiO}_2$  nanotubes anodized in electrolytes with different  $\text{NH}_4\text{F}$  concentrations. *Electrochim. Acta* **2015**, *176*, 1083–1091. [[CrossRef](#)]
96. Mazzarolo, A.; Curioni, M.; Vincenzo, A.; Skeldon, P.; Thompson, G.E. Anodic growth of titanium oxide: Electrochemical behaviour and morphological evolution. *Electrochim. Acta* **2012**, *75*, 288–295. [[CrossRef](#)]
97. Matykina, E.; Montuori, M.; Gough, J.; Monfor, F.; Berkani, A.; Skeldon, P.; Thomson, G.E.; Habazaki, H. Spark anodising of titanium for biomedical applications. *Int. J. Surf. Eng. Coat.* **2006**, *84*, 125–133. [[CrossRef](#)]
98. Diamanti, M.V.; Pedefferri, M.P. Effect of anodic oxidation parameters on the titanium oxides formation. *Corros. Sci.* **2007**, *49*, 939–948. [[CrossRef](#)]